Defense Threat Reduction Agency
8725 John J. Kingman Road, MS
6201 Fort Belvoir, VA 22060-6201

DTRA-TR-10-46

TECHNICAL REPORT

Thermal History Using Microparticle Trap Luminescence

Approved for public release; distribution is unlimited

June 2012

HDTRA01-07-1-0016

Joseph J. Talghader

Prepared by:
University of Minnesota
240 Williamson Hall
231 Pillsbury Drive S.E.
Minneapolis, MN 55455

DESTRUCTION NOTICE:

Destroy this report when it is no longer needed.
Do not return to sender.

PLEASE NOTIFY THE DEFENSE THREAT REDUCTION AGENCY, ATTN: DTRIAC OP-ONIU, 8725 JOHN J. KINGMAN ROAD, MS-6201, FORT BELVOIR, VA 22060-6201, IF YOUR ADDRESS IS INCORRECT, IF YOU WISH THAT IT BE DELETED FROM THE DISTRIBUTION LIST, OR IF THE ADDRESSEE IS NO LONGER EMPLOYED BY YOUR ORGANIZATION.

REPORT DOCUMENTATION PAGE

Form Approved
OMB No. 0704-0188

Public reporting burden for this collection of information is estimated to average 1 hour per response, including the time for reviewing instructions, searching existing data sources, gathering and maintaining the data needed, and completing and reviewing this collection of information. Send comments regarding this burden estimate or any other aspect of this collection of information, including suggestions for reducing this burden to Department of Defense, Washington Headquarters Services, Directorate for Information Operations and Reports (0704-0188), 1215 Jefferson Davis Highway, Suite 1204, Arlington, VA 22202-4302. Respondents should be aware that notwithstanding any other provision of law, no person shall be subject to any penalty for failing to comply with a collection of information if it does not display a currently valid OMB control number. **PLEASE DO NOT RETURN YOUR FORM TO THE ABOVE ADDRESS.**

1. REPORT DATE *(DD-MM-YYYY)*	2. REPORT TYPE	3. DATES COVERED *(From - To)*
00-06-2012	Technical	

4. TITLE AND SUBTITLE
Thermal History Using Microparticle Trap Luminescence

5a. CONTRACT NUMBER
HDTRA01-07-1-0016

5b. GRANT NUMBER

5c. PROGRAM ELEMENT NUMBER

6. AUTHOR(S)

5d. PROJECT NUMBER

5e. TASK NUMBER

5f. WORK UNIT NUMBER

7. PERFORMING ORGANIZATION NAME(S) AND ADDRESS(ES)
University of Minnesota

8. PERFORMING ORGANIZATION REPORT NUMBER

9. SPONSORING / MONITORING AGENCY NAME(S) AND ADDRESS(ES)
Defense Threat Reduction Agency
8725 John J. Kingman, STOP 6201
Ft. Belvoir, VA 22060-6201

10. SPONSOR/MONITOR'S ACRONYM(S)

11. SPONSOR/MONITOR'S REPORT NUMBER(S)
DTRA-TR-10-46

12. DISTRIBUTION / AVAILABILITY STATEMENT
Approved for public release; distribution is unlimited.

13. SUPPLEMENTARY NOTES

14. ABSTRACT
The primary objective of the grant was to investigate a thermal sensing technology and associated materials that extract thermal profiles from explosions in agent defeat test using micro- and nanoparticle trap luminescence. The number of occupied traps in a ceramic varies dynamically with temperature. Therefore, if the traps in a microparticle are filled prior to an agent defeat test using deep UV light or ionizing radiation, then the trap luminescence afterwards is a probe of the thermal history of the test.

15. SUBJECT TERMS
Luminescence Electrons
Microparticle Microheater

16. SECURITY CLASSIFICATION OF:			17. LIMITATION OF ABSTRACT	18. NUMBER OF PAGES	19a. NAME OF RESPONSIBLE PERSON
Unclassified			SAR	73	Mike Robinson
a. REPORT	b. ABSTRACT	c. THIS PAGE			19b. TELEPHONE NUMBER *(include area code)*
Unclassified	Unclassified	Unclassified			703-767-3076

Contents

1 EXECUTIVE SUMMARY

This report describes the research performed under DTRA grant HDTRA1-07-1-0016, "Thermal History using Microparticle Trap Luminescence" under Principal Investigators Joseph Talghader of the University of Minnesota and Eduardo Yukihara of Oklahoma State University during the period of December 1, 2006 – May 31, 2010.

The primary objective of the grant was to investigate a thermal sensing technology and associated materials that extract thermal profiles from explosions in agent defeat tests using micro- and nanoparticle trap luminescence. The number of occupied traps in a ceramic varies dynamically with temperature. Therefore, if the traps in a microparticle are filled prior to an agent defeat test using deep UV light or ionizing radiation, then the trap luminescence afterwards is a probe of the thermal history of the test.

The program was successful in all of its major components: concept demonstration, materials research, and preliminary explosive testing. The laboratory simulation of explosive heating was performed using micromachined heaters capable of reaching hundreds of degrees in milliseconds or less and cooling back to room temperature with arbitrary profiles. Among the successful concept demonstrations was one using Mg_2SiO_4:Tb,Co particles with two thermoluminescent peaks heated over a 232 °C to 313 °C range on time scales of less than 200 ms. The effect of maximum temperature during excitation on the intensity ratio of the two luminescent peaks was compared with first-order kinetics theory and shown to match within an average error of 4.4%.

In materials, lithium fluoride and natural topaz were identified as potential temperature sensing luminescent materials. A new luminescent ceramic, Mg_2SiO_4:Tb,Co was also found. This material has two traps of widely different energy depths within the band gap (with a weaker central third level). TL measurements show it can determine peak temperature over a range of roughly 150°C to 400°C. However, it appears susceptible to optical bleaching. Oxyorthosilicate nanophosphors were also investigated.

Preliminary explosive testing was performed in collaboration with Jim Lightstone at Indian Head Naval Surface Warfare Center. Thermoluminescent (TL) Al_2O_3:C microparticle sensors were demonstrated to survive detonation of pentaerythritol tetranitrate (PETN) high explosives. SEM imaging revealed only slight shape modification during an explosive event. Chemical analyses showed small increases in carbon and decreases in aluminum indicating Al combustion. Finally, the TL emission peak and shape remain stable to within 1.9% and 4.0% respectively, less than experimental error. This means that the ability of the particles to preserve thermal history information, were largely unaffected by detonation.

List of people involved in the project over the duration of the grant:

1. Joseph J. Talghader, Professor, University of Minnesota (PI)
2. Eduardo G. Yukihara, Associate Professor, Oklahoma State University (Co-PI)
3. Merlin Mah, Graduate Student, UM
4. Michael Manfred, Graduate Student, UM
5. Sangho Kim, Graduate Student, UM

6. Nick Gabriel (advisory), Graduate Student, UM
7. Juan Mittani, Postdoctoral Fellow, OSU
8. Victor Orante, Postdoctoral Fellow, OSU
9. Gregoire Denis, Postdoctoral Fellow, OSU
10. Daniel Temesgen, Graduate Student, OSU
11. Ojani Vega, Undergraduate Student, OSU
12. Noriyuki Masuda, Undergraduate Student, OSU
13. James Hazelton, Undergraduate Student, OSU
14. James Kelly, Undergraduate Student, OSU

Publications:

1. M. L. Mah, M. E. Manfred, S. S. Kim, M. Prokic, E. G. Yukihara, J. J. Talghader, "Measurement of rapid temperature profiles using thermoluminescent microparticles," *IEEE Sensors*, vol. 10, no. 2, February 2010, pp. 311-315.
2. M. Manfred, N. Gabriel, E. G. Yukihara, J. J. Talghader, "Thermoluminescence Measurement Technique using Millisecond Temperature Pulses,"*Radiation Protection Dosimetry*, vol. 139, no. 4, 2010, pp. 560-564.
3. E. G. Yukihara, L. G. Jacobsohn, M. W. Blair, B. L. Bennett, S. C. Tornga, and R. E. Muenchausen. "Luminescence properties of Ce-doped oxyorthosilicate nanophosphors and single crystals." J. Lumin. (in press, 2010).
4. J. R. Hazelton, E. G. Yukihara, L. G. Jacobsohn, M. W. Blair, and R. Muenchausen. "Feasibility of Using Oxyorthosilicates as Optically Stimulated Luminescence Detectors". Radiat. Meas. 45, 681-683 (2010).
5. M. W. Blair, L. G. Jacobsohn, S. C. Tornga, O. Ugurlu, B. L. Bennet, E. G. Yukihara, and R. E. Muenchausen. "Nanophosphor aluminum oxide: luminescence response of a potential dosimetric material". J. Lumin. 130, 825-831 (2010).
6. M. W. Blair, L. G. Jacobsohn, B. L. Bennett, S. C. Tornga, E. G. Yukihara, E. A. McKigney, and R. E. Muenchausen. "Luminescence and structural properties of oxyorthosilicate and Al_2O_3 nanophosphors". phys. status solidi c 206(5), 904-909 (2009).
7. J. C. Mittani, M. Prokić, and E. G. Yukihara. "Optically stimulated luminescence and thermoluminescence of terbium-activated silicates and aluminates". Radiat. Meas. 43, 323-326 (2008).

Conference presentations:

1. M. L. Mah, M. E. Manfred, S. S. Kim, M. Prokic, E. G. Yukihara, J. J. Talghader, "Sensing of thermal history using thermoluminescent microparticles," *2009 IEEE Optical MEMS and Nanophotonics Conference*, Clearwater, Florida, August 2009, pp. 23-24.
2. M. Manfred, M. Mah, N. Gabriel, E. G. Yukihara, and J. Talghader, "Pulsed Thermal Excitation of Luminescent Microparticles for Radiation Dosimetry," *2008 IEEE/LEOS Optical MEMS and Nanophotonics Conference*, Freiburg Germany, August 2008, pp. 64-65.
3. J. R. Hazelton, E. G. Yukihara, M. W. Blair, L. G. Jacobsohn, R. Muenchausen. "Feasibility of using oxyorthosilicates as optically stimulated luminescence radiation detectors." 7th International Conference on Luminescent Detectors and Transformers of Ionizing Radiation, LUMDETR-2009, Kraków, Poland, July 12th – 17th (2009).
4. E. G. Yukihara, L. G. Jacobsohn, M. W. Blair, B. L. Bennett, S. C. Tornga, R. E. Muenchausen. "Thermally and Optically Stimulated Luminescence of Nanophosphors Prepared by Solution Combustion Synthesis". 15th International Conference on Luminescence and Optical Spectroscopy of Condensed Matter. Lyon, France, July 7-11 (2008).
5. L. G. Jacobsohn, M. W. Blair, B. L. Bennett, S. C. Sitarz, R. E. Muenchausen, N. Masuda, E. G. Yukihara. "Thermoluminescence Properties of Gd_2SiO_5:Ce Nanophosphor Prepared by Solution Combustion Synthesis". 16th International Conference on Defects in Insulating Materials, Aracaju, Brazil, August 24-29 (2008).
6. J. C. Mittani, M. Prokic, and E. G. Yukihara. "Optically stimulated luminescence and thermoluminescence of terbium-activated silicates and aluminates". 15th Solid State Dosimetry Conference, Delft, The Netherlands, July 8-13 (2007).

2 INTRODUCTION

When a cache of biological weapons is destroyed, every region containing infectious particles must be brought to a minimum thermal profile to insure sterilization. Unfortunately, the extreme violence of an agent defeat simulation prohibits existing temperature sensors from functioning. In this report, the investigation of a thermal sensing technology is described that extracts thermal profiles from the luminescence of ceramic microparticles, particularly oxides with high band gaps. The number of occupied traps in a ceramic varies dynamically with temperature. Therefore, if the traps in a microparticle are filled prior to an agent defeat test using deep UV light, then the trap luminescence afterwards is a probe of the thermal history of the test.

This approach, which is schematically shown in Figure 1, has several advantages:

a) The particles themselves have no parts that can be damaged by the agent defeat test; they are merely implanted quartz or similarly tough ceramics that can easily withstand the harshest environments and procedures.
b) The materials are usually very cheap.

c) The particles can be micromachined to take on just about any shape or size, and thus will have essentially identical aerodynamics and thermal experience to the bioagents that they simulate.
d) Fluctuations in the thermal history can be seen from the differences in luminescence from region to region or even particle to particle.
e) The luminescence data is exponentially weighted towards the highest temperatures experienced, which are the most critical in destroying infectious agents.
f) Extreme thermal profiles, such as those seen in agent defeat tests, can be simulated using micromachined heaters that increase temperature to hundreds of degrees and cool in less than a millisecond.
g) The luminescence of the particles is largely independent of particle size unlike methods based on quantum size effects or phase change. This means that precise control of size is not critical during materials fabrication.

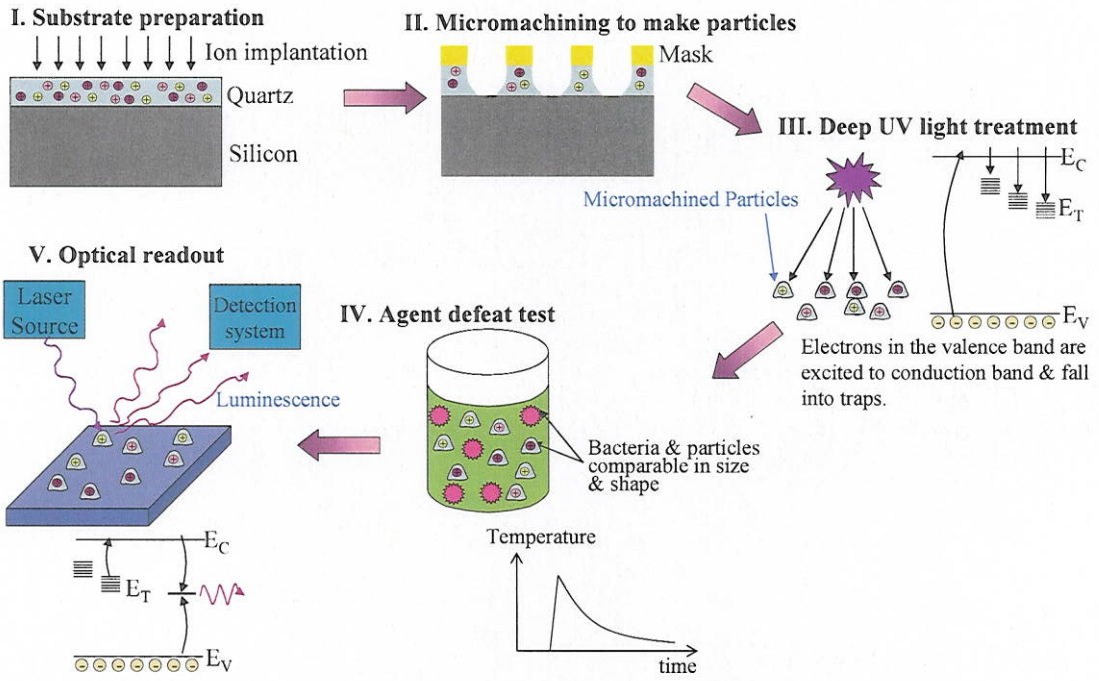

Figure 1 – Measuring the thermal history of an agent defeat test using microparticle luminescence. The ceramic particles are micromachined to match the size and shape of bacterial or viral agents and dispersed in a burst vessel. After the test, luminescence from the microparticles is measured to extract the temperature experienced in any region of the system.

3 METHODOLOGY

3.1 Thermoluminescence Testing and Apparatus

The simulation of explosive heating without using explosives and the analysis of particles after an agent defeat test both required a new method of luminescent analysis. Microheaters were

ideal for these as they were easy to fabricate, had extremely short time constants, and could be ramped to any temperature below their degradation points with the application of a relatively small current.

There could be commercial dual-use possibilities for microheater-driven TL testing as well. Many radiation dosimetry measurements currently use badges that contain Al_2O_3:C particles whose trap levels fill based on the radiation dose received. These badges are then periodically sent to a central laboratory to be tested. If the Al_2O_3:C could be heated in pulses with microheaters with an integrated avalanche photodiode, one might be able to obtain real-time analysis of radiation dose. This is the subject of a recent patent disclosure of the UM/OSU collaboration.

Figure 2a is a scanning electron microscope (SEM) image of a row of microheaters from early in the program. They were fabricated in a standard micromachining process using a polysilicon resistor sandwiched between two LPCVD nitride layers. Contact to the poly was made using an RIE etch and Cr/Au metallization.

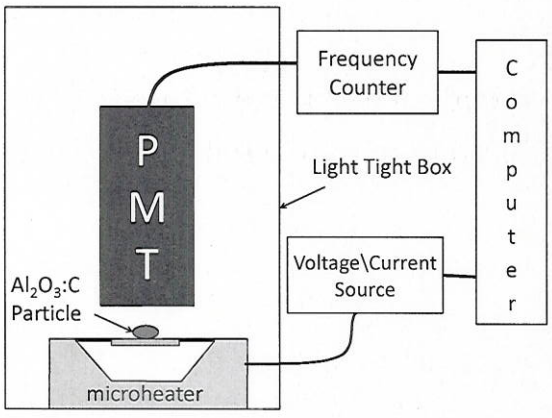

Figure 3 – Diagram of experimental set-up. The system requires very little complexity. A photomultiplier tube (PMT) is placed in proximity to the microheater and connected to a counter. A current source drives the microheater.

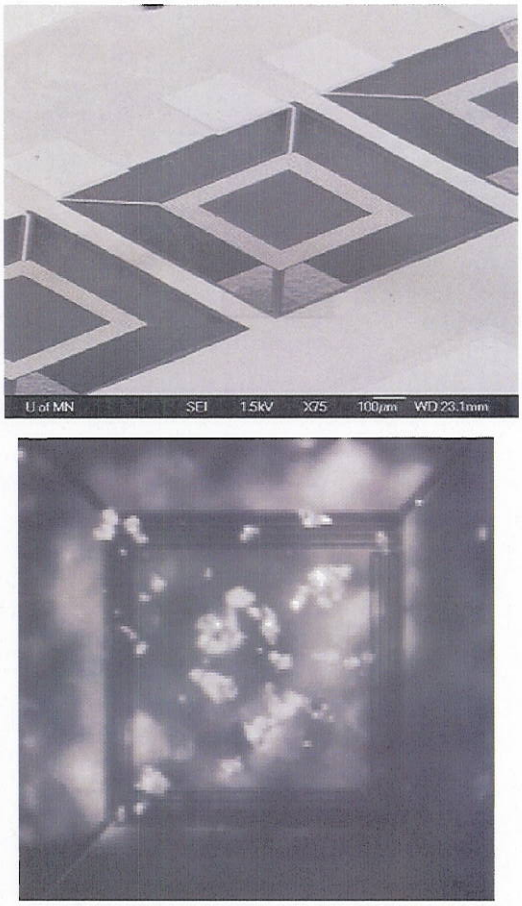

Figure 2 – Images of early microheaters. a) (top) shows an SEM image of the microheaters after fabrication. b) (bottom) shows an optical micrograph of the heaters after Al_2O_3:C particles have been dispersed across them.

A KOH etch was used for release. Figure 2b shows an optical image of the device with Al_2O_3:C particles on it.

The temperature coefficients of resistance (TCR) of the polysilicon resistors were determined by heating the chip containing the devices using a thermoelectric device and measuring the resistance changes with temperature. These data were only taken over a small range but the validity of the TCR data to higher temperatures (~400°C) was strongly supported by the linearity of the 1/R vs. I^2 plot used to determine the microheater thermal conductance.

Figure 3 shows a diagram of an early

experimental setup. After Al_2O_3:C particles were placed on the heaters, the particles were exposed to UV radiation to fill the traps. The most readily accessible source was a deep-UV lamp of λ=205nm, but for radioactive testing, a β-decay source could be used. After irradiation, the current to the microheaters was gradually increased. We estimated a heating rate of 2°C/second. As the particles were heated they emit light whose intensity is related to the radiation dose they have received. The peak of the TL is indicative of the depth of the traps within the bandgap.

In the second and third years, we completely automated our basic thermoluminescence (TL) measurement system. A particle of TL material can now be placed on a microheater, and once the computer control is activated, the traps can be filled by UV light, an explosive heating cycle can be performed, a TL ramp can be performed, and then the cycle can be repeated as often as necessary to obtain the full relationship between thermal history and luminescence. Figures 4, 5, 6, and 7 below show the system details.

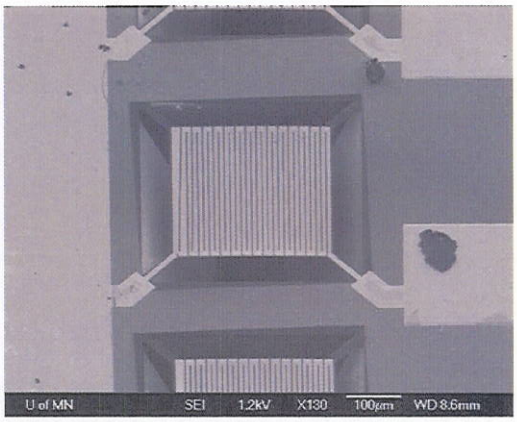

Figure 4 – A microstructure used for heating the luminescent microparticles at rates simulating agent defeat explosions.

At the core of our thermoluminescence curve collection setup is a microheater (Figure 4) consisting of a 150nm-thick platinum resistor sputtered on 1nm adhesion layer of chrome, in turn on a 200nm LPCVD nitride; silicon wet-etching makes this a platform suspended above a ~300µm-deep pit. The linear temperature vs. resistance relationship of the resistor is found by measuring its resistance while heating it on a hotplate. The microheater is driven by a Keithley 2410 sourcemeter for linear heating ramps or a HP 8114A pulse generator for explosive heating. Particle luminescence is measured by a Electron Tubes Ltd. P25PC photomultiplier tube and BK Precision 1823A frequency counter; the radiation for filling sample traps is provided by a deuterium lamp putting out 0.8 mW/cm^2 of 180-400nm UV light. A motorized aluminum shutter provides protection for the PMT during irradiation. (Figures 5-7).

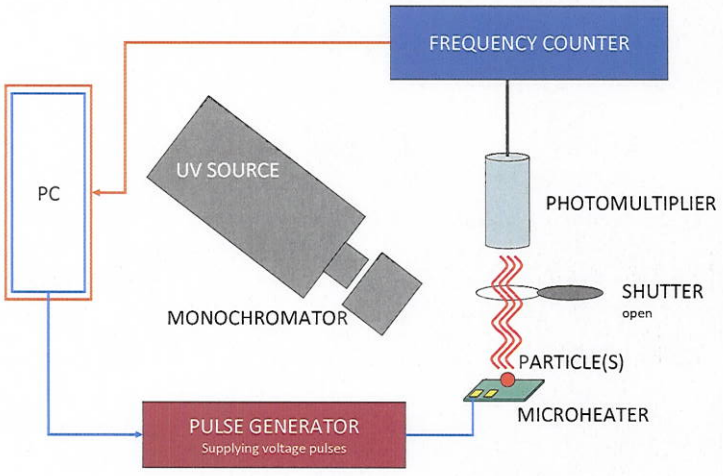

Figure 5 – Conceptual diagram of experimental apparatus.

The script for an explosively-heated thermoluminescence experiment is to first fill the traps via UV irradiation, then explosively heat the sample via voltage pulse to the microheater. A linear heating ramp then follows to induce and measure thermoluminescence. For

normalization and consistency checking purposes, a non-pulsed TL reference curve is sometimes collected before the traps are refilled for the main pulsed experiment.

A number of custom Python programs coordinate and control most of the thermoluminescence measurement process. This allows the experiment to run, automated and remotely-controlled, inside a blacked-out darkroom admitting an average measured background light signal of around 600 counts per second (including the photomultiplier's quoted 200 CPS dark count rate). The recent addition of feedback sensing to many experiment parts provides enhanced stability and confidence of precision. Resulting data is processed mainly using MATLAB.

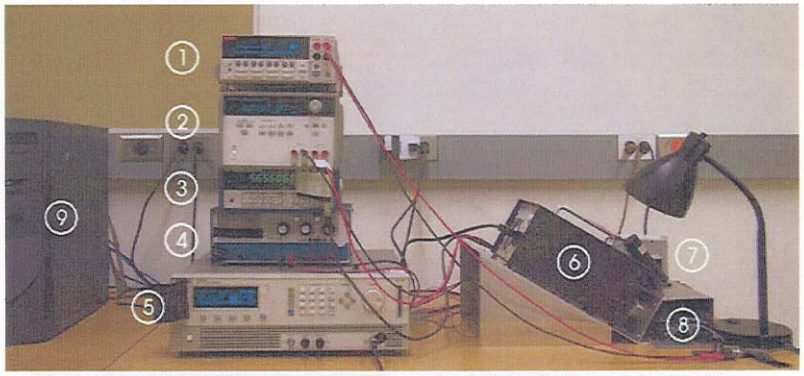

1. Keithley 2410 sourcemeter drives microheaters for linear ramp
2. Agilent E3647A DC supply computer controlled power for PMT
3. BK Precision 1823A frequency counter tracks PMT counts
4. Heathkit TP-2718 DC supply powers stepper control circuit
5. HP 8114A pulse generator for microheater explosive heating
6. UV source gives 180-400 nm light for sample irradiation
7. LED darkroom bulb for handling light-sensitive samples
8. Microprobe positioners connect to microheater contacts
9. PC controls 1-6 above for automated/remote operation

Figure 6 – Photograph of the control electronics of the thermoluminescence excitation, and testing system.

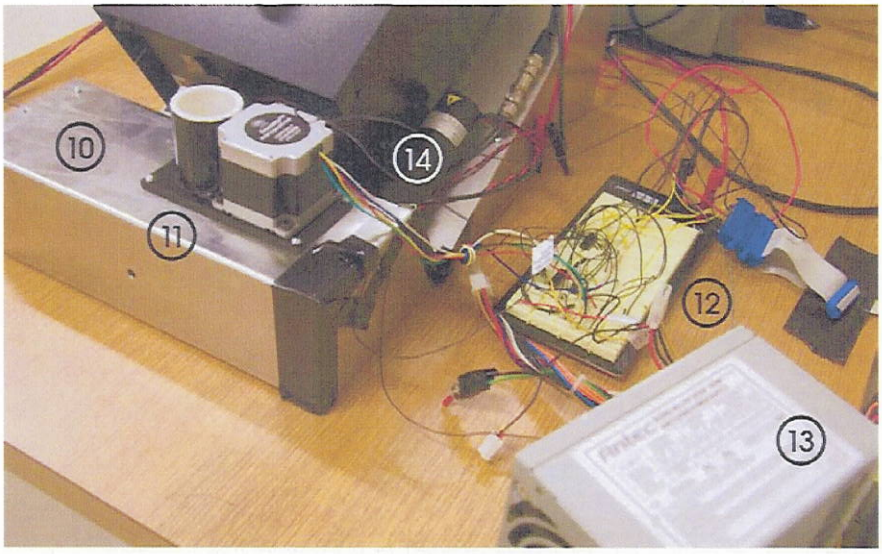

10. Custom sample chamber holds UV source, PMT, and shutter assembly in place
11. Stepper motor moves aluminum shutter (inside chamber) with position sensing
12. Stepper motor control circuit translates PC commands to shutter movement
13. PC power supply provides high currents required by stepper motor
14. Electron Tubes P25PC PMT high-sensitivity light detection for thermoluminescence

Figure 7 - Shuttering system and sample chamber for microheaters.

Obviously, one cannot perform actual agent-defeat testing in a university setting. In order to eliminate the need to explode particles, we perform much of our thermoluminescent testing on

micromachined heaters. These devices are fabricated using VLSI techniques and are essentially dielectric plates with integrated metal or semiconductor resistors. The time constants of these heaters vary from several tens of microseconds to hundreds of milliseconds depending on their size and thermal isolation. Figure 8 shows the Temperature versus Input Power for a heater than is directly connected to its substrate. The time constant for this device is about 100μs, which is even faster than one expects in the periphery of an agent defeat event. Figure 9 shows an SEM image of a device of this type. (Of course, in the center of an agent defeat event, the heat transfer time will be even faster than this because the transfer is mediated by radiation; however, the peak temperatures in a radiation-limited environment are so high that no infectious agents would survive anyway.)

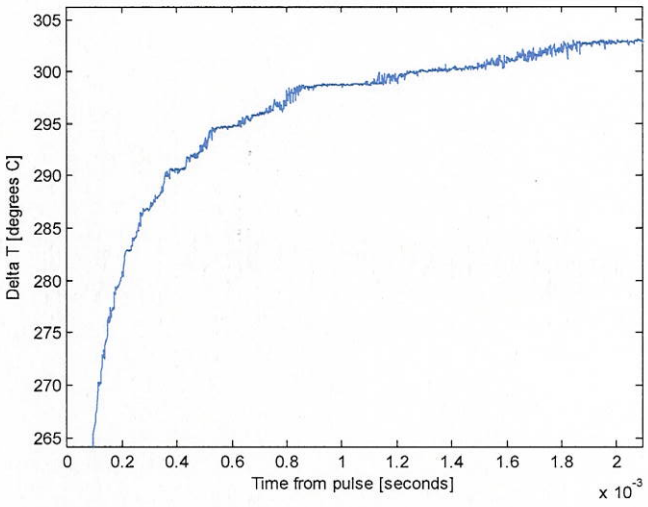

Figure 8 – Timing diagram of a microheater similar to that shown Figure 6. Note that the time to reach 275°C is less than 200μs.

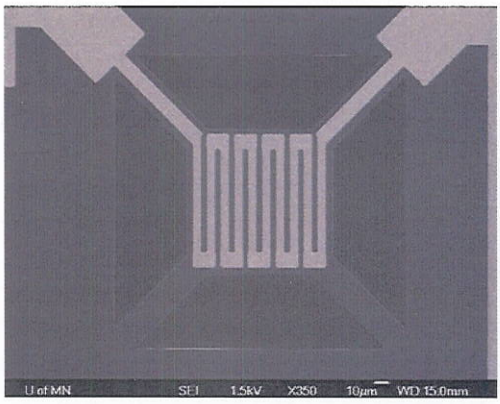

Figure 9 – High speed microheater. This heater has a short time constant because it is directly connected to the substrate; however, it cannot reach the temperatures of released heaters without damage.

Figure 10 shows the Temperature versus Power curves for a microheater whose substrate has been etched out from underneath it. This type of microheater can be heated to hundreds of degrees assuming the dielectrics and metals/semiconductors have been chosen properly. The time constant of such microheaters is generally in the tens of milliseconds, which is sufficient for most explosive heating simulations and is certainly capable of distinguishing between different levels of a slow cool-down.

Figure 11 shows a potential pitfall of microheaters if they are not designed properly: nonuniform heating. This problem was seen in the first year microheaters but was subsequently remedied by insuring that the heating resistors ran through every portion of the heaters. Images of such heaters are shown in Figure 9 and in the results sections. Another potential pitfall is ensuring that the particle thermal mass is not larger than that of the microheater. Otherwise, the particle temperature will not follow the heater temperature.

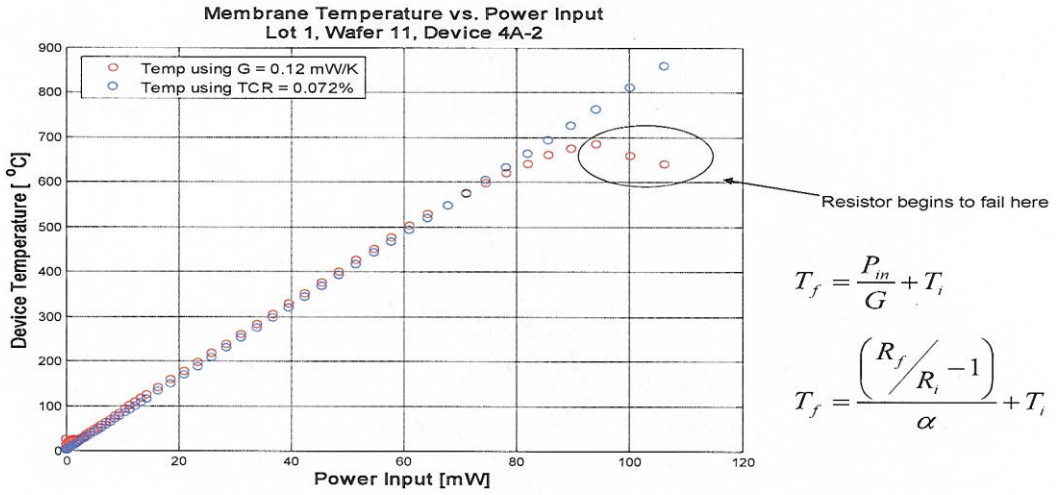

Figure 10 – Temperature vs. Power for a released microheater.

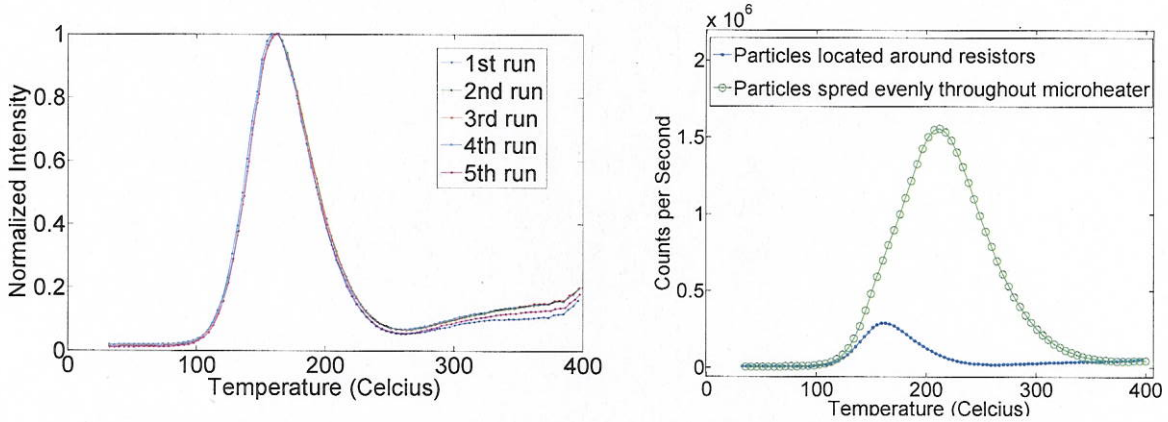

Figure 11 – Repeatability and variability in early microheater TL. On the left, Figure (a) shows that a microparticle on a heater that is excited by deep UV light repeatedly and tested repeatedly in the same position. It has extremely stable TL characteristics. On the right, however, particles are tested on different regions of a microheater. Particles located near the heating resistors on the microheaters are apparently exposed to higher temperatures than particles located away from them. Based on these results, we redesigned our heaters to have resistors that covered every region on the heater for temperature uniformity so that all particles gave the same TL regardless of location.

3.2 Samples

This project included the characterization of existing materials (commercially available or obtained through collaborators), and experimental characterization of materials synthesized in our laboratory at Oklahoma State University. Table 1 lists the materials investigated in this project, the synthesis process used to produce them, and the source of the material (if not synthesized in the laboratory).

Table 1. List of materials characterized for potential use as temperature sensors.

Material	*Synthesis process*	*Source*
Dosimetric materials		
Al_2O_3:C	Crystal growth	Landauer Inc.
LiF:Mg,Ti	Crystal growth	Thermo Fisher Scientific Inc.
Artificial materials		
$LiAlO_2$	Sintering	Institute of Nuclear Sciences, Belgrade, Serbia
Mg_2SiO_4	Sintering	Institute of Nuclear Sciences, Belgrade, Serbia
$CaSiO_3$	Sintering	Institute of Nuclear Sciences, Belgrade, Serbia
Y_2SiO_5:Ce (YSO)	Crystal Growth	Los Alamos National Laboratory
Gd_2SiO_5:Ce (GSO)	Crystal Growth	Hitachi Chemical Co., Ltd.
Lu_2SiO_5:Ce (LSO)	Crystal Growth	Los Alamos Natinal Laboratory
Y_2SiO_5:Ce (YSO)	SCS	Los Alamos National Laboratory
Gd_2SiO_5:Ce (GSO)	SCS	Los Alamos National Laboratory
Lu_2SiO_5:Ce (LSO)	SCS	Los Alamos National Laboratory
Al_2O_3	SCS	
$Li_2B_4O_7$	SCS	
MgO	SCS	
La_2O_3	SCS	
$LaAlO_3$	SCS	
$LaMgO_3$	SCS	
$MgAl_2O_4$	SCS	
$LaMgAl_{11}O_{19}$	SCS	
CeO_2	SCS	
Natural materials		
$Al_2SiO_4(F,OH)_2$ (topaz)	Natural	
Al_2SiO_5	Natural	

3.3 Material synthesis

Samples were synthesized at Oklahoma State University using the Solution Combustion Synthesis (SCS) technique (Chick et al., 1990; Kingsley and Patil, 1988; Kingsley et al., 1990; Yen and Weber, 2004). The reagents were dissolved in water, dried in a hot plate at 200°C for ~1-2 h. The temperature of the hot plate was then increased to 500°C until combustion occurred (~7 min). The remaining powder was collected, crushed in a agate mortar, and annealed (typically at 900°C for 2 h) to remove organic residuals and promote growth of the crystallites. Doped materials were investigated by adding the dopant (e.g. $Ce(NO_3)_3{\cdot}6H_2O$) in the initial solution in the desired amount. Figure 12 illustrates the stages of the SCS process and Table 2 lists the materials synthesized, typical quantities used in the synthesis, and dopants investigated.

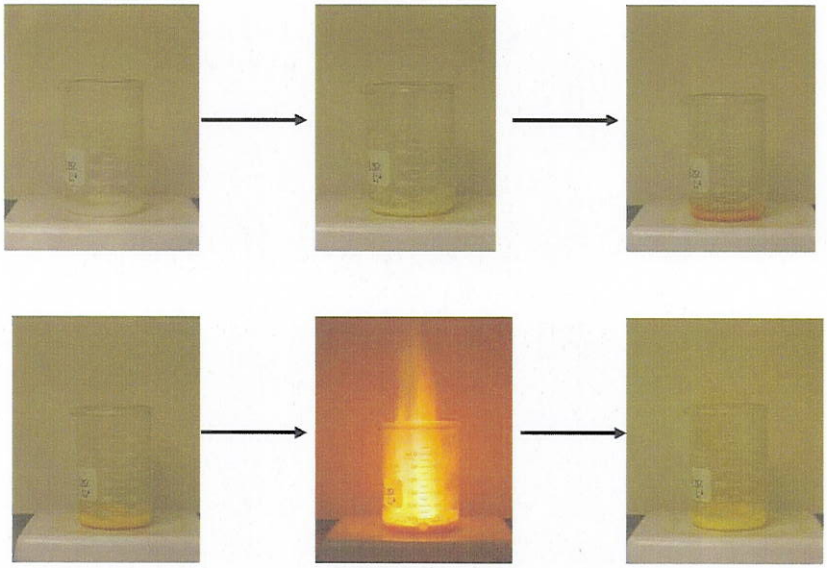

Figure 12. Stages of the Solution Combustion Synthesis process. The first photo shows the material after the 1 h drying, after which the hot plate temperature was increased to 500°C and the other photos were obtained. Combustion is seen ~6 min after raising the temperature of the hot plate.

Table 2. Materials synthesized by SCS and dopants investigated.

Material	*Reagents*	*Dopants*
Al_2O_3	5 g $Al(NO_3)_3{\cdot}9H_2O$, 2.0 g $(NH_2)_2CO$ (urea); 18.7 g $Al(NO_3)_3{\cdot}9H_2O$, 6.25 g $C_2H_5O_2N$ (glycine)	Ce, Er, Li
$Li_2B_4O_7$	10.2 g NH_4NO_3, 2.47 g H_3BO_3, 3.69 g Li_2CO_3, 7.65 g $(NH_2)_2CO$ (urea)	Ce, Eu
MgO	12.8 g $Mg(NO_3)_2{\cdot}6H_2O$, 5 g $(NH_2)_2CO$ (urea); 12.8 g $Mg(NO_3)_2{\cdot}6H_2O$, 4.166 g $C_2H_5O_2N$ (glycine); 12.8 g $Mg(NO_3)_2{\cdot}6H_2O$, 2.086 ml $C_2H_5O_2N$ (ethylenediamine);	Ce, Er, Li, Tm, Yb, Tb, Eu
La_2O_3	21.6 g $La(NO_3)_2{\cdot}6H_2O$, 7.5 g $(NH_2)_2CO$ (urea)	Ce, Li
$LaAlO_3$	11.5 g $La(NO_3)_2{\cdot}6H_2O$, 10 g $Al(NO_3)_3{\cdot}9H_2O$, 4 g $(NH_2)_2CO$ (urea)	Ce
$LaMgO_3$		
$MgAl_2O_4$	5g $Al(NO_3)_3{\cdot}9H_2O$, 1.71 g $Mg(NO_3)_2{\cdot}6H_2O$, 2.675 g $(NH_2)_2CO$ (urea);	Ce, Er
$LaMgAl_{11}O_{19}$	2.1 g $Al(NO_3)_3{\cdot}9H_2O$, 1.24 g $Mg(NO_3)_2{\cdot}6H_2O$, 20 g $Al(NO_3)_3{\cdot}9H_2O$, 9.2 g $(NH_2)_2CO$ (urea);	Ce
CeO_2	10.8 g $Ce(NO_3)_2{\cdot}6H_2O$, 3.75 g $(NH_2)_2CO$ (urea)	Eu, Li

3.4 Equipment

3.4.1 Radioluminescence (RL) measurements

RL measurements were performed using a Magnum X-Ray tube (Moxtek, Orem, USA) operating under 40 kVp with W filament and Ag target. All measurements were made using 100 μA tube current, which results in a dose rate of approximately 150 mGy/s. The RL was detected using a USB-2000 miniature fiber optic spectrometer (Ocean Optics), equipped with a ILX511 linear silicon CCD array (Sony) and a fixed polymer rule grating allowing a 700 nm dispersion range with maximum efficiency at 500nm. The luminescence is guided from the sample toward the spectrometer using an optical fiber (1 mm core diameter, transmission between 200 – 1100 nm) and a f/2 fused silica lens to couple the sample luminescence to the optical fiber. The spectrometer has an order-sorting detection filter to eliminate the second order interference light and ~7.2 nm resolution.

3.4.2 Thermoluminescence (TL)

TL measurements were performed using a Risø TL/OSL-DA-15 reader. Irradiations were carried out using the integrated $^{90}Sr/^{90}Y$ beta source delivering a dose rate of ~100 mGy/s. The TL was detected using an Electron Tubes 9235QB photomultiplier tube with optical filters in front of it to select specific emission bands. Typical filters used are Schott BG-39 for visible detection (6 mm total thickness, Schott AG, Mainz, Germany) and Hoya U-340 filters for UV detection (7.5 mm total thickness, Hoya Corporation, Tokyo, Japan). Nitrogen gas was purged in the sample chamber for the TL measurements to avoid spurious luminescence.

3.4.3 X-ray diffraction

X-ray diffraction data was obtained using a Phillips Analytical X-ray PW3020 with Cu Kα radiation by scanning the 2θ in 0.02 degrees step size and 0.5 s scan step time.

4 RESULTS

4.1 Modeling the Effect of Thermal History on Idealized Materials

In this section, we briefly examine the ability of ideal first order materials to distinguish time and temperature in a rapid thermal event. The next section will discuss real luminescent materials and section 4.3 will cover actual experimental demonstration of temperature sensing in rapid thermal events.

The ultimate goal of using microparticle thermoluminescence for thermal history sensing is to be able to extract the entire history, not just maximum temperature. Further one wishes to be able to distinguish extremely rapid changes. The first step towards this ultimate goal is to independently be able to isolate maximum temperature and cooling time. (Note that heating rate is extremely fast in explosions and therefore plays less of a role in the total energy delivered to an object or biological particle than T_{max} and cooling rate.) The following discussion shows that

a variety of Tmax and cooling combinations can give identical results in a TL curve. For example, consider that the periphery of an explosion has a maximum temperature of 800K and cools over 10 seconds. This thermal history would cause a shallow trap in a TL material to empty but a deeper trap may still be populated this leads to a specific population ratio. If this is the only pair of traps used then an explosion with (T_{max} = 800K, cooling = 10 seconds) may give the same TL results as an explosion with (T_{max} = 810K, cooling = 5 seconds). However, if one uses three or more traps, one can specify both T_{max} and cooling time by looking at the data from two or more different trap population ratios.

A single first-order trap--i.e. one combination of s and E--which undergoes an explosive heating event of a given maximum temperature and duration with initial electron population n_0 may afterward host a certain population of still-trapped electrons. Under first-order kinetics theory, for each possible value of one thermal event parameter (either maximum temperature or cooling rate), there is a single value of the other which will result in exactly the same surviving population. If the difference between the population number resulting from an "actual", pre-determined explosive heating event and those from another set of explosion parameters are plotted on the plane of explosive heating and duration variables, the result is a one-to-one curve along which the match is exact, indicating that the explosive heating event could have possessed any pair of parameters lying along this "correctness curve". Given one of the explosive heating event's two distinguishing values, the other can be found.

The correctness curve, shown in 3D and contour views in Figures 13 and 14, were calculated from two traps subjected to a simulated explosive heating event reaching to 300 °C and lasting for 5 seconds. A similar but not identical profile is shown in Figure 15. This set of parameters can indeed be found on the line along which the correctness is 100%, i.e. where the actual remaining population of the traps--the only information about the explosion that the producing simulation is given--matches that predicted by theory. For visualization purposes, we have found it easiest to calculate the percent error between the "actual" explosive heating event parameters

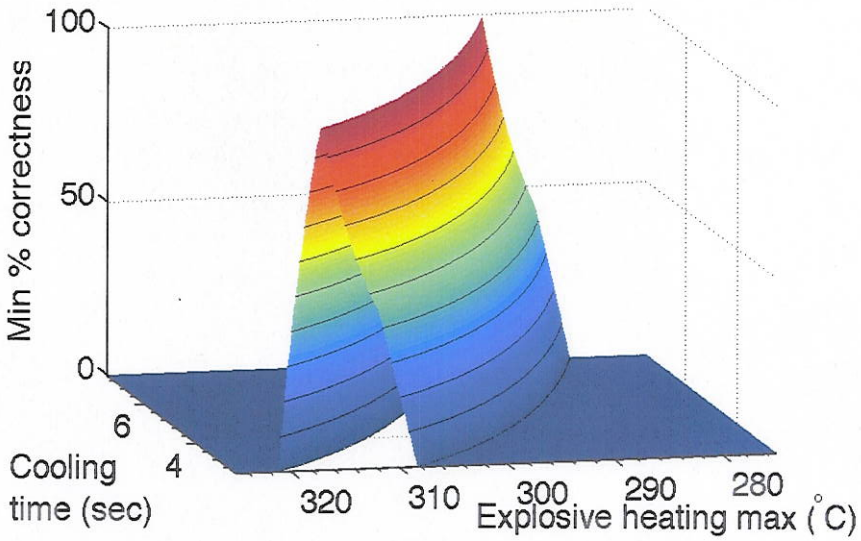

Figure 13 – Correctness curve that represents how identical TL signatures may be obtained from different combinations of maximum temperature and cooling. The "correctness" is defined by how well the population ratio of two peaks (for example the two MgSiO4:TbCo peaks in Figure 4) matches that of one specific Tmax/cooling time combination. Note that many combinations with lead to identical TL results if only one particle or pair of peaks is used.

and the candidates being considered, cap large error values at 100%, and then to subtract these from unity to yield what we term the "percent correctness".

To provide a reference thermoluminescence level with which to counteract the effects of varying overall luminescence from observation to observation, another trap may be added and the ratio between the two glow curve peaks' heights used instead of the absolute intensity. Therefore, two traps of suitably differing parameters will in theory enable the experimental recovery of a single explosive heating parameter--either maximum temperature or duration--if the other parameter is already known.

Changing the trap parameters causes the shape of the correctness curve to change. In order to reconstruct the thermal event without first knowing either parameter, we can therefore introduce additional traps to undergo the same heating; if the trap characteristics are different enough, the resulting lines determining the explosive heating

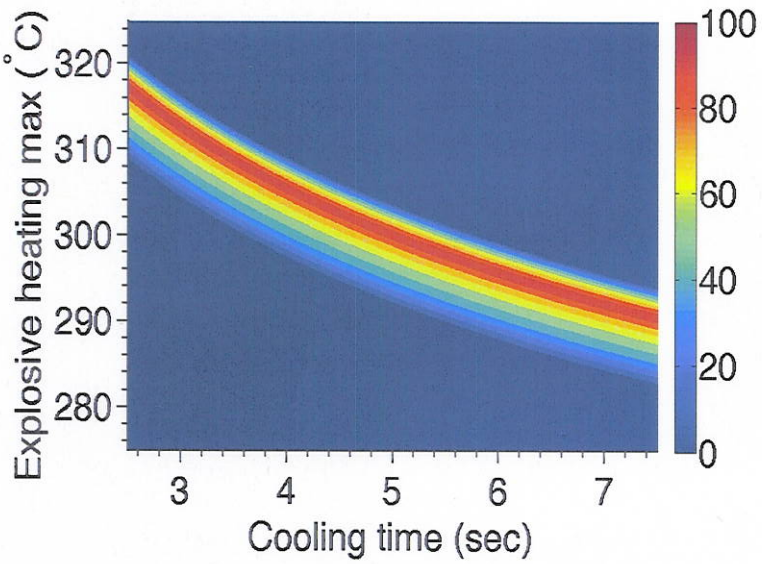

Figure 14 – Contour plot of "correctness curve" that represents how identical TL signatures may be obtained from different combinations of maximum temperature and cooling. The "correctness" is defined by how well the population ratio of two peaks (for example the two MgSiO4:TbCo peaks in Figure 4) matches that of one specific Tmax/cooling time combination. Note that many combinations with lead to identical TL results if only one particle or pair of peaks is used.

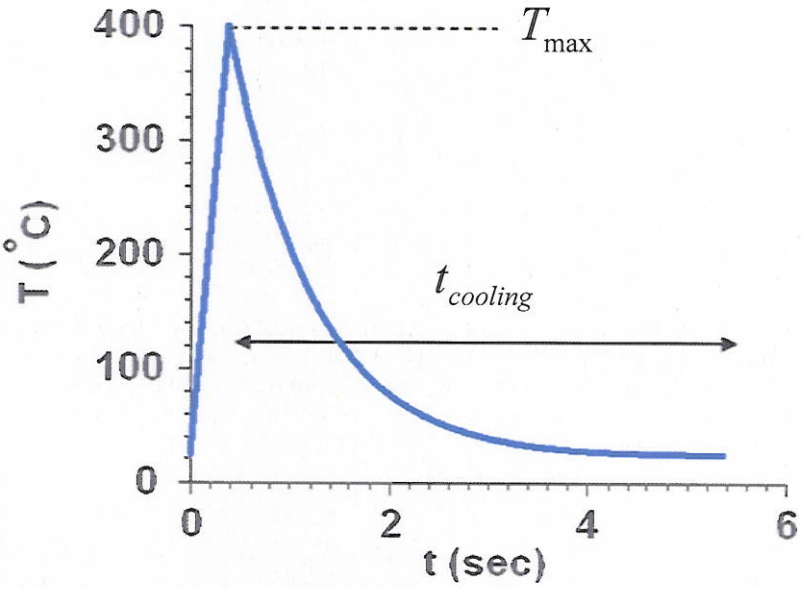

Figure 15 – Heating profile to simulate an explosive event. A rapid linear heating ramp bring the temperature to 400°C in a few milliseconds. Afterwards a slow cooling over several seconds brings the temperature back to ambient.

parameters that each trap's (or pair of traps') results deem possible intersect, giving us a single set of candidates to describe the explosive heating.

The overlaid correctness curves of three pairs of traps subjected to the same thermal heating event reaching to 300°C and lasting for 5 seconds. Subsequent calculation using only knowledge of the trap parameters and the pre- and post-explosion electron populations, as can be gathered by experiment, reveals that the intersection of the three correctness curves indicates a single possible thermal event description: a maximum temperature of 300°C and a duration of 5 seconds. By using two correctness curves and a single shared reference trap, the same result can be achieved with just three traps, although some tuning of their parameters is necessary.

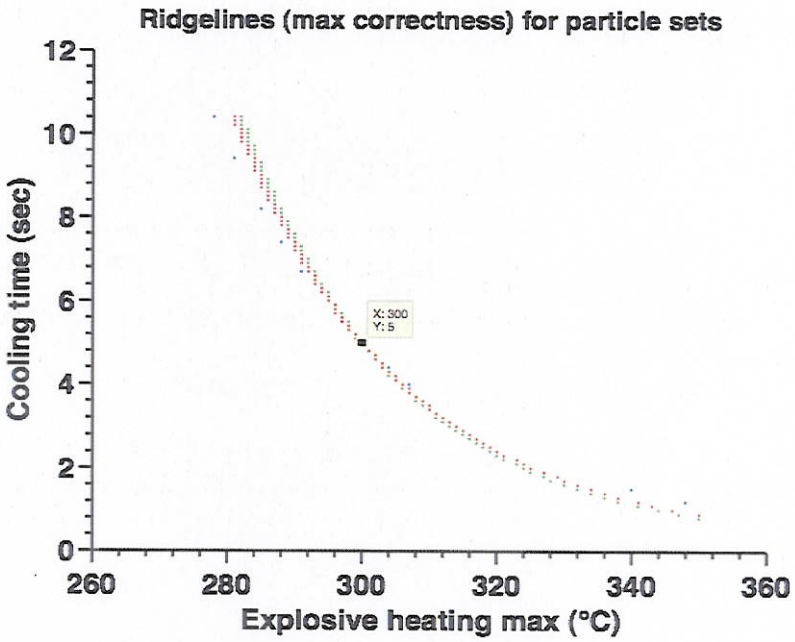

Figure 16 – Diagram showing two contour plots from two pairs of traps with similar characteristics. Note that even these relatively similar trap pairs give independent curves with a well-defined intersection that can identify the true maximum temperature and cooling time of an agent-defeat event.

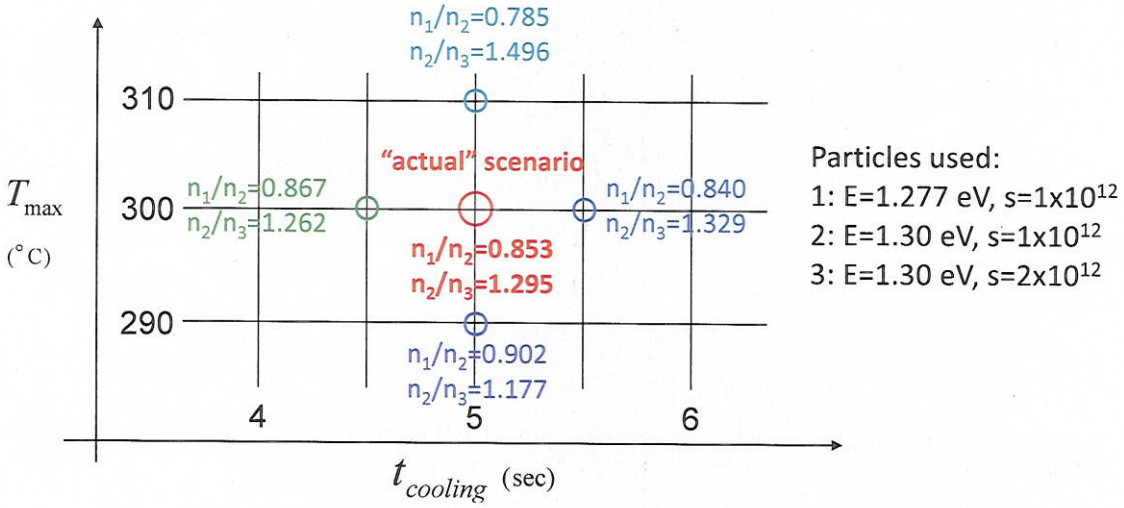

Figure 17 – This graph shows the ratios of three traps with different characteristics (trap depth and phonon interaction frequency, shown at right) under the influence of different heating conditions. Note that one can distinguish both time and temperature under these conditions. The traps are *not* the same as those simulated in Figure 16.

4.2 Modeling the Effect of Thermal History on Luminescence Materials

The behavior of real luminescence materials with thermal history or pre-heating temperature is dependent not only on the maximum temperature, but on the time-temperature profile. To determine the thermal history during explosive events, it is necessary to develop an understanding on how much the heating and cooling rates affect the population of trapped charges.

To develop this understanding, we simulated a material with three trapping levels at different depths below the conduction band, which after irradiation produces the hypothetical TL curve shown in Figure 18. Each one of these TL peaks provides information on a specific temperature range.

The effect of pre-heating on the TL curve is shown in Figure 19a. As the maximum pre-heating temperature increases, the intensity of the TL peaks decrease sequentially because the corresponding trapped charges are emptied. The intensity of the TL peaks is plotted against the maximum temperature in Figure 19b. The range in which the peaks decrease is the useful temperature range that can be "probed" by each TL trap.

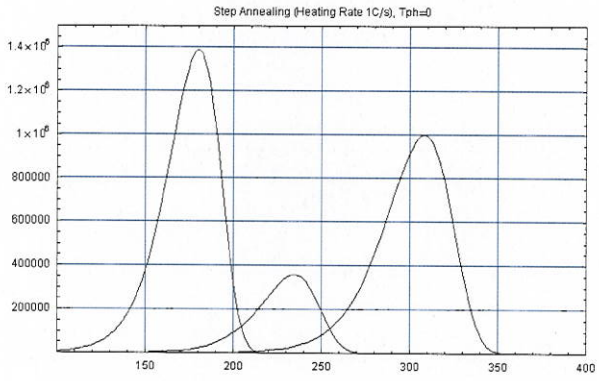

Figure 18. TL curve of a hypothetical material containing three trapping levels at depths 1.19 eV, 1.33 eV, and 1.53 eV. The frequency factor was assumed to be 10^{12} s^{-1} and the heating rate was 1°C/s.

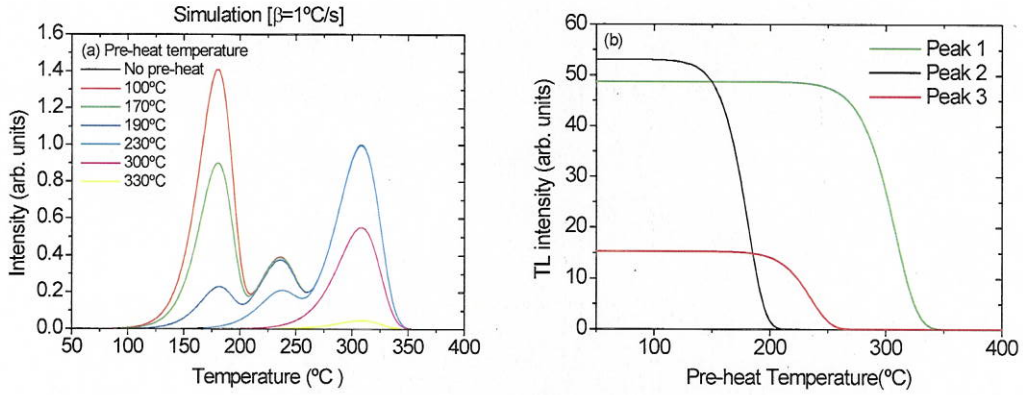

Figure 19. Effect of maximum pre-heating temperature on: (a) the TL curve of a hypothetical material with three trapping levels; (b) the maximum intensity of the TL peaks.

However, the "useful" temperature range of each TL trap depends in general on the heating rate. Therefore, we simulated how the traps are emptied by pre-heatings applied at various heating rates, from 0.1 K/s to 500 K/s. The trap population is plotted against the maximum pre-heat temperature in Figure 20.

As the heating rate of the thermal history increases, the detrapping profile shifts to higher temperatures and becomes less dependent on heating rate. Therefore, in the case of a fast rise in temperature characteristic of an explosion, the population of trapped electrons will depend only on the maximum temperature, and not on the heating rate.

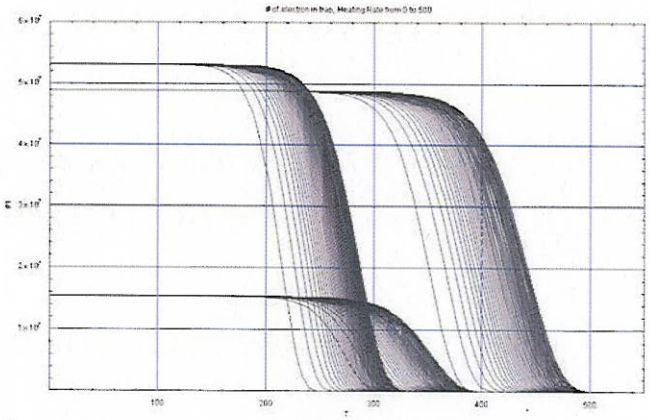

Figure 20. Trap population *versus* maximum pre-heat temperature for heating rates from 0.1 K/s up to 500 K/s.

The simulations carried out so far indicated that the possibility of determining the maximum thermal history temperature is more feasible for fast heating rates (explosion) than for slow ones, but one has to keep in mind the "useful" temperature range of each trapping center. However, the simulations assume an instantaneous cooling to room temperature. Influence of the cooling rate will be discussed in the next section.

4.2.1 Test of TL models

The investigations involved in the development of temperature sensing using TL materials require modeling of the TL process. These models can be useful to understand the influence of extremely fast heating rates or to predict the effect of different temperature profiles in the TL curves. In this section, we analyzed the curve of a standard TL material (LiF:Mg,Ti) using a superposition of first-order TL peaks (Randall and Wilkins, 1945) and investigated whether the first-order model is capable of reproducing the effect of temperature to which the material was exposed on the TL curves.

We are particularly interested in this study in using a model obtained from TL data recorded at low heating rate and apply the model to TL data recorded at a higher heating rate. The goal is to extrapolate this approach in the future for the extremely fast heating rates experienced during explosive events.

4.2.1.1 The first-order TL model for multiple peaks

The first-order TL model assumes that trapping centers do not interact, *i.e.*, the trapped electron escaping the trap recombines immediately with the hole resulting in luminescence. For a single type of defect characterized by an activation energy E and frequency factor s, the rate of change in the concentration of trapped charges n is given by (McKeever, 1985):

$$\frac{dn}{dt} = -nse^{-E/kT}. \tag{1}$$

This equation can be integrated to obtain the number of trapped charges at any instant t when the material is subjected to a temperature profile:

$$n(t) = n_0 \exp\left[-s\int_0^t e^{\frac{E}{kT(t)}}dt\right]. \tag{2}$$

In this equation, n_0 is the initial concentration of charges in the trapping centers.

During a TL readout, the TL intensity (s^{-1}) is proportional to the rate of recombination. In *quasi-equilibrium* (charges escaping the trap recombine immediately), the TL intensity can be written as:

$$I_{TL}(t) = \left|\frac{dm}{dt}\right| = \left|\frac{dn}{dt}\right| = nse^{-E/kT}. \tag{3}$$

For a linear heating rate such that $T(t) = T_0 + \beta t$, Eq. (2) can be written as

$$n(T) = n_0 \exp\left[-\frac{s}{\beta}\int_{T_0}^{T}\exp\left(-\frac{E}{k\theta}\right)d\theta\right]. \tag{4}$$

The TL intensity in K^{-1} then becomes:

$$I(T) = \frac{n_0 s}{\beta}e^{\frac{E}{kT}}\exp\left[-\frac{s}{\beta}\int_{T_0}^{T}\exp\left(-\frac{E}{k\theta}\right)d\theta\right]. \tag{5}$$

This is the well-known first-order TL model, first proposed by Randall and Wilkins (1945).

Some important properties of the first-order TL processes are the following:

(a) In presence of multiple first-order processes, each process can be treated independently and the total TL intensity is a superposition of the TL intensity due to each process;

(b) The peak temperature does not depend on the initial trap occupancy, *i.e.*, the absorbed dose in the crystal.

Condition (a) allows us to write the following equation for a material containing multiple TL peaks, the i-th peak characterized by E_i and s_i:

$$I(T) = \sum_i \frac{n_{0,i} s_i}{\beta} e^{-\frac{E_i}{kT}} \exp\left[-\frac{s_i}{\beta} \int_{T_0}^{T} \exp\left(-\frac{E_i}{k\theta} \right) d\theta \right]. \tag{6}$$

4.2.1.2 A formalism to describe the effect of a heating profile

In this study we assume that, previously to the TL readout, the material is subjected to a heating profile in which the temperature is elevated from an initial temperature T_0 until a maximum temperature T_m at a constant rate α (K s^{-1}), and then decreases exponentially with a time constant τ until it reaches the initial temperature T_0. This temperature profile can be written as

$$\theta(t) = \begin{cases} T_0 + \alpha t & \text{if } t < t_m \\ T_0 + (T_m - T_0) e^{-\frac{t - t_m}{\tau}} & \text{if } t > t_m \end{cases}. \tag{7}$$

where we define t_m as the instant in which the temperature reaches a maximum.

According to Eq. (2), the concentration of trapped charges after the material returns to the initial temperature, n'_0, is

$$n'_0 = n_0 \exp\left[-s \int_0^{t_m} e^{-\frac{E}{kT(t)}} dt - s \int_{t_m}^{\infty} e^{-\frac{E}{kT(t)}} dt \right]. \tag{8}$$

The exponential term can be factored into two terms, one expressing the fraction of trapped charges released during heating, $f = f(E, s, T_m, \alpha)$, and one expressing the trapped charges released during cooling, $g = g(E, s, T_m, \tau)$. Using the temperature profile given in Eq. (6), this can be written as

$$n'_0 = n_0 f(E, s, T_m, \alpha) g(E, s, T_m, \tau), \tag{9}$$

where

$$f(E, s, T_m, \alpha) = \exp\left[-\frac{s}{\alpha} \int_{T_0}^{T_m} e^{-\frac{E}{k\theta}} d\theta \right] \tag{10}$$

and

$$g(E, s, T_m, \tau) = \exp\left[-s\tau \int_{T_0}^{T_m} \frac{e^{-\frac{E}{k\theta}}}{\theta - \theta_0} d\theta \right]. \tag{11}$$

Therefore, the effect of the temperature profile is to reduce the original concentration of trapped charges by a factor f during the heating stage times a factor g during the cooling stage.

For a material containing a superposition of first-order TL peaks, the effect of the temperature profile to which the material was exposed prior to the TL readout is to reduce each peak by a factor $f_i g_i$, where the sub-index i refers to a particular TL peak, *i.e.*, to a particular set of E_i and s_i values. The total TL intensity is then given by

$$I(T) = \sum_i f_i g_i \frac{n_{0,i} s_i}{\beta} e^{-\frac{E_i}{kT}} \exp\left[-\frac{s_i}{\beta} \int_{T_0}^{T} \exp\left(-\frac{E_i}{k\theta} \right) d\theta \right]. \tag{12}$$

4.2.1.3 Experimental tests

Experimental TL data was obtained using LiF:Mg,Ti dosimeters of dimensions 3 mm × 3 mm × 0.9 mm. A 4-mm thick Kopp 5850 filter and a 3-mm thick HA3 filter were used in front of the PMT to reduce the blackbody radiation and transmit the main luminescence band from LiF:Mg,Ti at 410-415 nm (McKeever et al., 1995). No annealing procedure was used in between experiments.

Deconvolutions of the TL curves into first-order TL peaks were carried out using PeakFit™ version 4 (Jandel Scientific Software) with a user-defined Randall-Wilkins model as in Eq. (5), the integral being approximated by (Chen and McKeever, 1997):

$$\int_{T_0}^{T} e^{-\frac{E}{k\theta}} d\theta \cong \frac{kT^2}{E} e^{-\frac{E}{kT}} \left(1 - \frac{2kT}{E} + \frac{6k^2T^2}{E^2} \right). \tag{13}$$

Numerical modeling was carried out using Mathematica 5.2 (Wolfram Research Inc.).

4.2.1.4 Analysis of the LiF:Mg,Ti TL curve

Figure 21 shows the TL curve of LiF:Mg,Ti recorded at a heating rate of 0.2 K/s. The curve was fitted with first-order TL peaks, resulting in the parameters shown in Table 3. As one can observe in Figure 21, the TL curve can be well-represented by a superposition of first-order TL peaks in a first approximation. The parameters obtained shown in Table 3 can now be used to predict the effect of an arbitrary temperature profile on the TL curves of this material using the formalism previously presented in this section. Here we restricted our investigations to the temperature profiles described by Eq. (7).

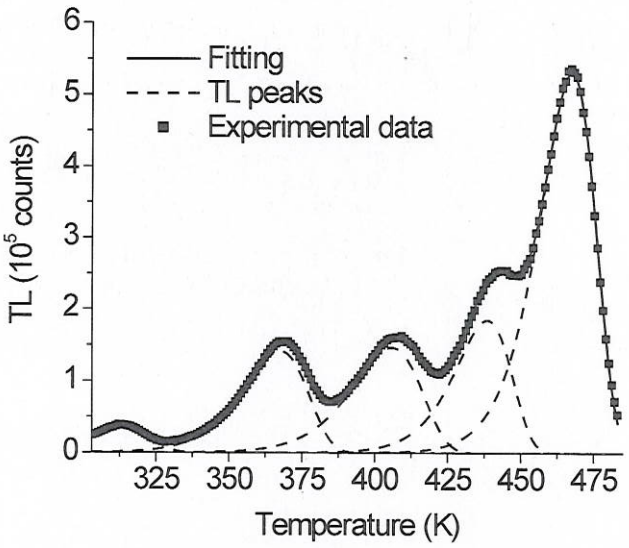

Figure 21. TL curve of LiF:Mg,Ti fitted with a superposition of first-order TL peaks (heating rate of 0.2 K/s; see fitted parameters in Table 3).

Table 3. Parameters obtained by fitting the TL curve of LiF:Mg,Ti with first-order TL peaks.

TL peak	*n_0 (arb. units)*	*E (eV)*	*s (s^{-1})*
Peak 1	1.19×10^{6}	0.740	1.19×10^{10}
Peak 2	4.60×10^{6}	1.042	2.91×10^{12}
Peak 3	5.11×10^{6}	1.182	6.68×10^{12}
Peak 4	5.15×10^{6}	1.698	5.64×10^{17}
Peak 5	1.44×10^{7}	1.962	2.61×10^{19}

4.2.1.5 Comparison of experimental and numerical simulations of TL curves

Figure 22 shows a comparison of experimental and simulated TL curves obtained immediately after irradiation or after irradiation and pre-heating to different temperatures (373 K, 423 K, and 473 K) at a heating rate of 5 K/s. Note that the heating rate used in the pre-heating and simulation is ~20 times faster than the heating rate used to record the data from which the model was based on (0.2 K/s). Cooling is assumed to be immediate in the case of both experiment and numerical simulations.

First of all, the results in Figure 22 shows the effect of the different effect of the pre-heating on the various TL peaks of LiF:Mg,Ti. The important point, however, is to note that the qualitative agreement between the model prediction (column on the right) with the experimental data (columns on the left). The implications is that, in spite of the oversimplified assumption of first-order behavior, the TL model based on data recorded at slow heating rate was able to predict the effect of a fast heating profile. It remains to be demonstrated whether this model also applies to

the extremely fast heating profiles experienced during explosive events and reproducible using the microheaters developed in this project.

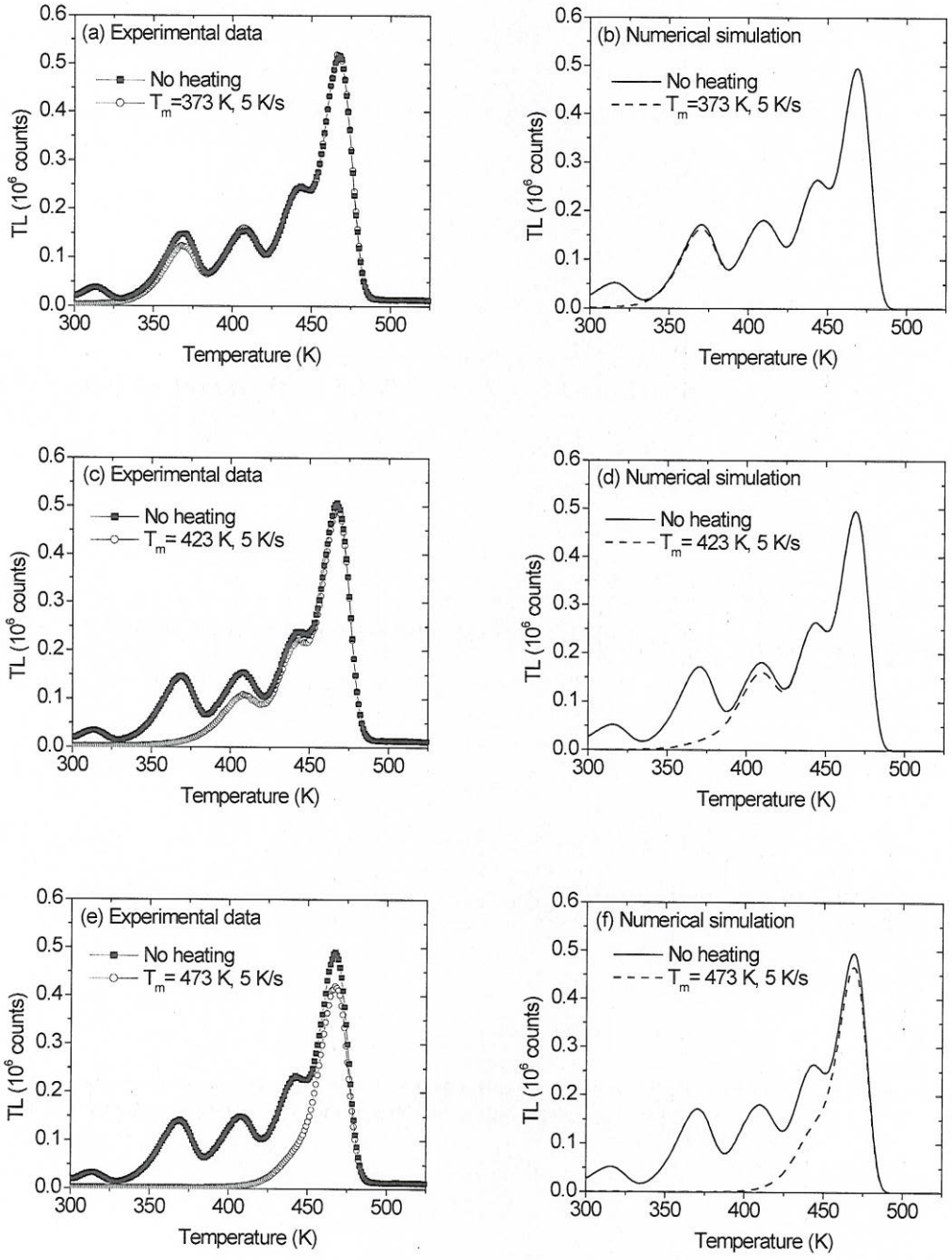

Figure 22. Experimental and simulated TL curves of LiF:Mg,Ti (heating rate of 0.2 K/s) immediately after irradiation or subjected to a pre-heating to different temperatures (373 K, 423 K, and 473 K) at a fast heating rate 5 K/s. The simulated curves are prediction of the effect of heating rate on the TL curves based on the first-order model parameters presented in Table 3.

4.2.1.6 Effect of different temperature profiles

One question that can be answered based on this model is if a superposition of TL peaks can distinguish between two different heating profiles that would affect one of the TL peaks in the same way. Consider for example a heating profile with maximum temperature of 443 K and heating rate of 2 K/s. Based on the data on Table 3 and the formalism developed earlier, such heating profile reduces TL peak 3 to 20% of its original value. A heating profile with maximum temperature of 406 K and heating rate of 0.1 K/s would also reduce TL peak 3 to 20% of its original value. This means that in a material with a single TL peak similar to peak 3, these two heating profiles could not be distinguished based on the TL curve.

However, with a superposition of TL peaks such as the one found in LiF:Mg,Ti, the numerical simulations shown in Figure 23a indicates that, although the effect of the two temperature profiles on peak 3 is identical, the effect on peak 4 is not. As a result, a difference in the TL curves can be observed around 443 K. Moreover, this prediction was confirmed by experimental data presented in Figure 23b, in which TL curves of LiF:Mg,Ti subjected to these two temperature profiles are compared with the TL peak when no pre-heating is applied. Again, a difference in the TL intensity can be observed around 443 K.

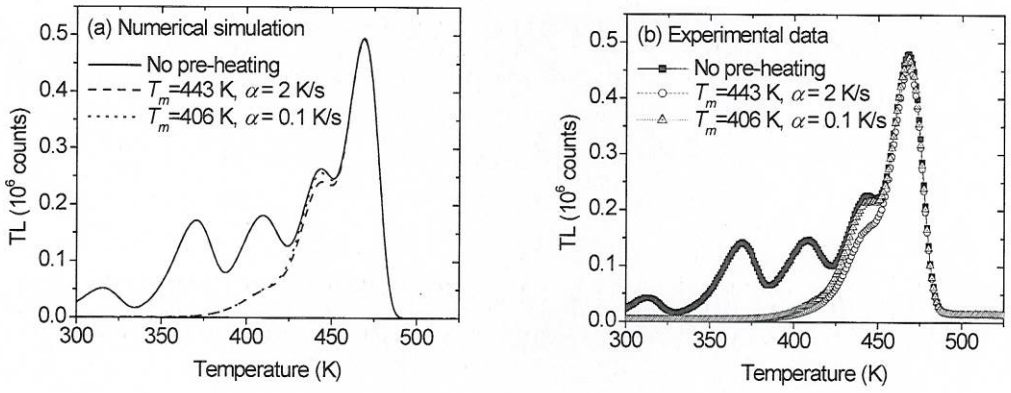

Figure 23. (a) Numerical simulation and (b) experimental data on the effect of two heating profiles (maximum temperature of 443 K at 2 K/s, and maximum temperature of 406 K at 0.1 K/s).

4.2.1.7 Influence of cooling stage

The discussion in the previous section does not include the effect of the cooling state. As one may expect, the cooling state will be important if cooling is slower than the heating stage. Here we establish a more precisely condition to whether the cooling state will or will not affect the temperature determination.

Comparing Eq. (10) and (11) one can see that the condition for the heating stage to be predominant is:

$$\frac{1}{\alpha} >> \frac{\tau}{T}, \qquad (14)$$

where T is in the range of temperatures in which we are interested. For example, for a slow heating rate of $\alpha = 1$ K/s and a slow cooling rate with time constant $\tau = 10$ s, the depletion is going to be dominated by the heating stage. For $\alpha = 1$ K/s and $T \sim 450$ K, this conditions reduces to $\tau << 450$ s. For a fast heating rate of $\alpha = 10^3$ K/s and $T \sim 450$ K, this conditions reduces to $\tau << 4.5$ s.

The model developed in the previous section can also be used to investigate the effect of cooling rate in the TL peaks. Figure 24 shows simulated TL curves of LiF:Mg,Ti heated to 443 K at a heating rate of 2 K/s, but in which the cooling constant τ assumed different values. According to the condition expressed by Eq. (13), the heating stage ceases to be dominant only when $\tau \sim$ 220 s. This is confirmed by the simulations presented in Figure 24, which shows that the cooling constant have no effect on the TL curves until it reaches a value ~300 s.

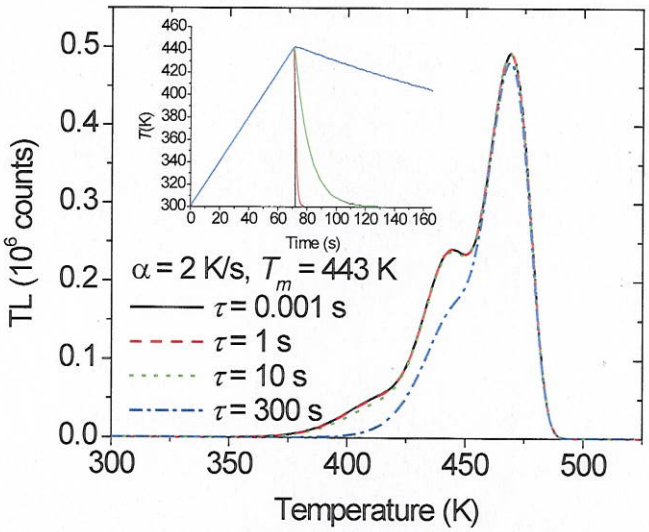

Figure 24. Numerical stimulation on the effect of cooling constant τ on the TL curves of LiF:Mg,Ti heated to 443 K at a heating rate of 2 K/s. The inset shows the various simulated temperature profiles to which the material was subjected.

4.2.2 Implementation of automated initial rise method

The model above demonstrates that it is possible to predict the effect of a fast heating profile using TL parameters (activation energy and frequency factor) obtained using a slow heating profile in laboratory. To obtain these parameters, the TL curve must be fitted with a set of TL peaks. One of the useful techniques to obtain the activation energies of a TL curve is to use a step-annealing technique and apply the initial rise method (McKeever, 1985). In this section we tested an automated analysis to apply the initial rise method.

The automated initial rise method analysis was implemented in Mathematica 5.2 and applied to a few materials. Figure 25 shows representative examples of TL curves obtained using partial cleaning (step-annealing) of the TL curves, which consists in heating to the specified temperature

to clean the low temperature TL peaks, followed by cooling to room temperature and measurement of the whole TL curve. This procedure subsequently empties the traps related to low temperature peaks, "exposing" the high temperature peaks. The application of the initial rise method to these curves allows one to find the activation energy for the trapping centers associated with peaks at increasing temperatures, therefore providing an "activation energy spectrum" for the TL in the material. One can see in Figure 25 that the automated method produced activation energies that are very similar to the manual analysis of the curves, although some discrepancies were observed for the YO sample (Figure 25b).

In order to test the reliability of this analysis procedure, we also simulated a material containing four first-order TL peaks (Figure 26). The simulated data was then treated as the experimental data and analyzed using the initial rise method. The results showed in Figure 27 demonstrate that under these ideal conditions the activation energies could be successfully recovered. However, in regions where the TL curves have low intensity, anomalous values of activation energies were obtained.

The conclusion is that an ideal situation is to materials with well-defined first-order TL peaks. This would make it easier to obtain the TL parameters and done for LiF:Mg,Ti in Section 4.4.2. If not possible, the approach described here could be used to extract the parameters for a large superposition of TL peaks.

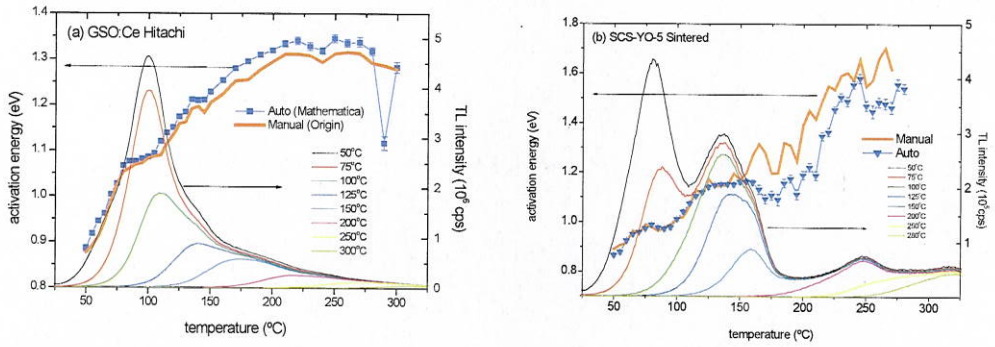

Figure 25. Application of initial rise method to Gd_2SiO_5:Ce and Y_2O_3 (undoped).

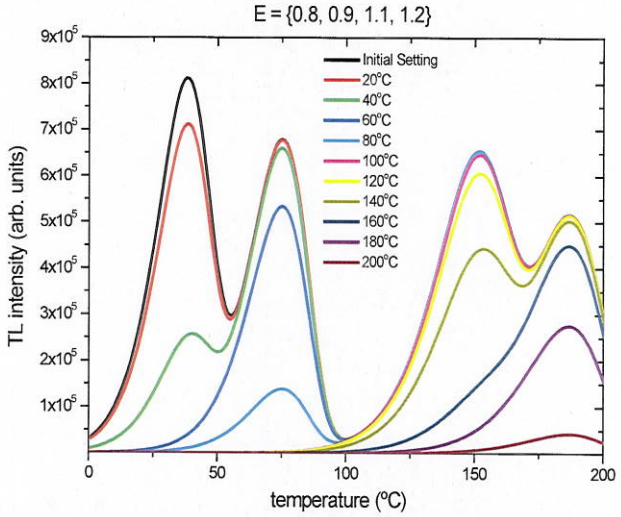

Figure 26. Simulated TL curve containing four peaks with activation energy of 0.8 eV, 0.9 eV, 1.2 eV and 1.2 eV.

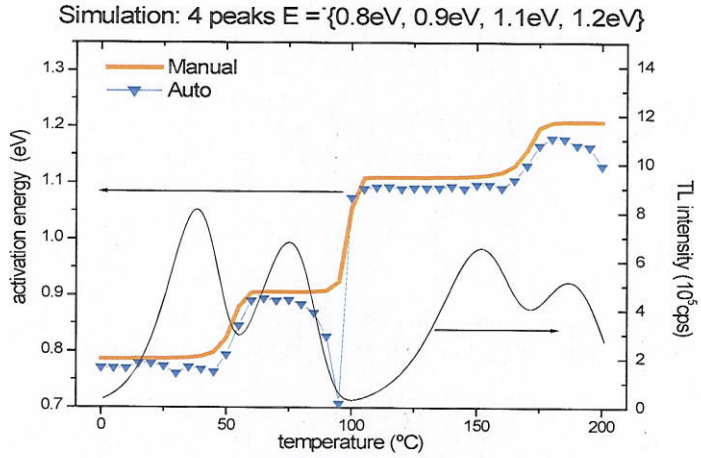

Figure 27. Activation energy recovered using the automated initial rise method and manual method.

4.3 Experimental Demonstration of Microparticle Thermal Sensors

4.3.1 Background

The investigation and demonstration of temperature sensing using thermoluminescent microparticles was primarily performed at the University of Minnesota by Ph.D. graduate student Merlin Mah under the direction of Professor Talghader with support from Professor Yukihara of OSU.

Thermoluminescent materials have extensive applications in radiation dosimetry (Escobar-Alarcon, 2003) and sedimentary dating (Wintle, 1979). In dosimetry, ionizing radiation excites electron-hole pairs in high bandgap materials, filling previously-empty electron traps; thermoluminescence (TL) is later used to assess their occupancy. In dating, background radiation from sediment fills the traps over time (the sun having emptied all traps prior to burial).

The lifetime of trapped charges is determined by the Arrhenius equation, which states the probability of detrapping per unit time as equal to s exp $(-E/kT)$, where s is a frequency factor measured in s^{-1}, E is the activation energy for the process, T is the temperature and k is the Boltzmann constant (McKeever, 1985). Since the Arrhenius relationship includes a strong variation with temperature, the luminescence of a material should also serve as a probe of the thermal history to which that material has been exposed. This concept has only previously been applied to natural TL materials in meteorites to determine their probable orbital distance prior to entry into Earth's atmosphere (McKeever, 1980)(Benoit, 1991)(Sears, 1974).

It is demonstrated in this paper that thermoluminescent materials can be used as active temperature sensors. Microparticles of TL materials are uniquely suited for the detailed profiling of extremely violent temperature events, such as the explosive destruction of biological particles, that would destroy existing direct-contact sensors. TL microparticles have no fabricated components, are often composed of highly robust materials, are inexpensive and relatively simple to fabricate in large quantities, can be micromachined to match the size and shape of a bioagent or to be injected into an otherwise-sealed system, and can be spread en masse in order to probe temperature differences in different spatial regions.

4.3.2 Microparticles and Microheaters

Mg_2SiO_4:Tb,Co (magnesium silicate) microparticles were chosen for having two or more well-separated thermoluminescence peaks occurring at conveniently reachable temperatures. Microparticles with diameters on the order of 10–20 μm were prepared (Mittani, 2008) by Dr. M. Prokic, Institute of Nuclear Sciences. They are sprinkled onto microheaters, as shown in Figure 28.

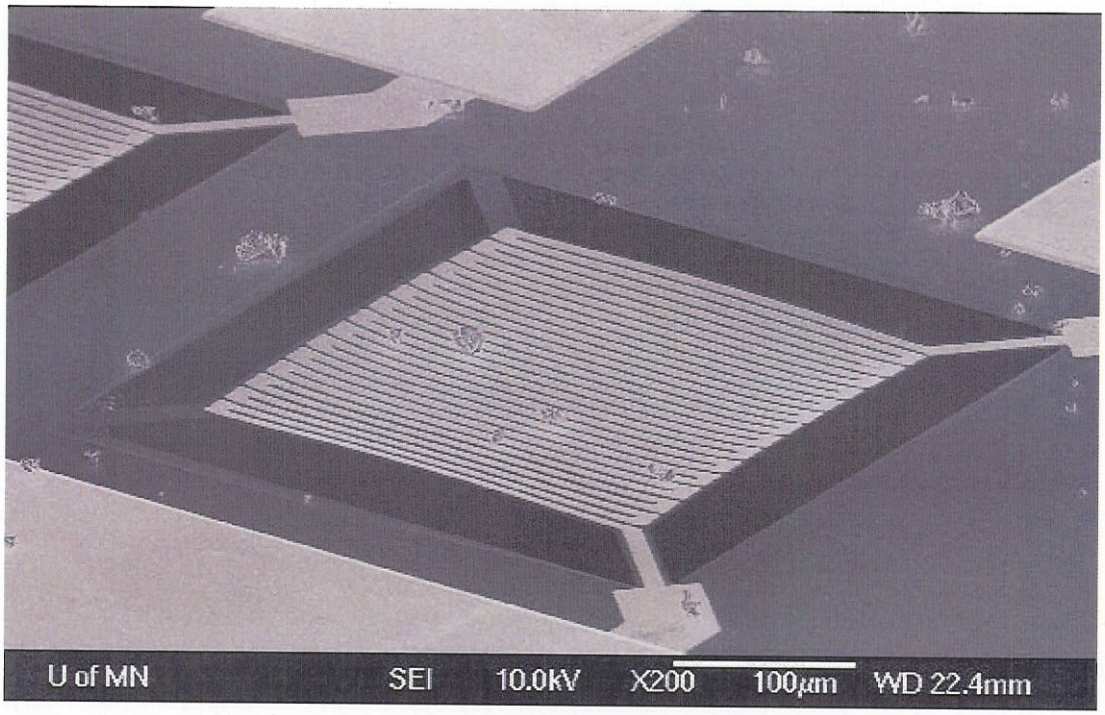

(a) A microheater topped with several Mg_2SiO_4:Tb,Co microparticles

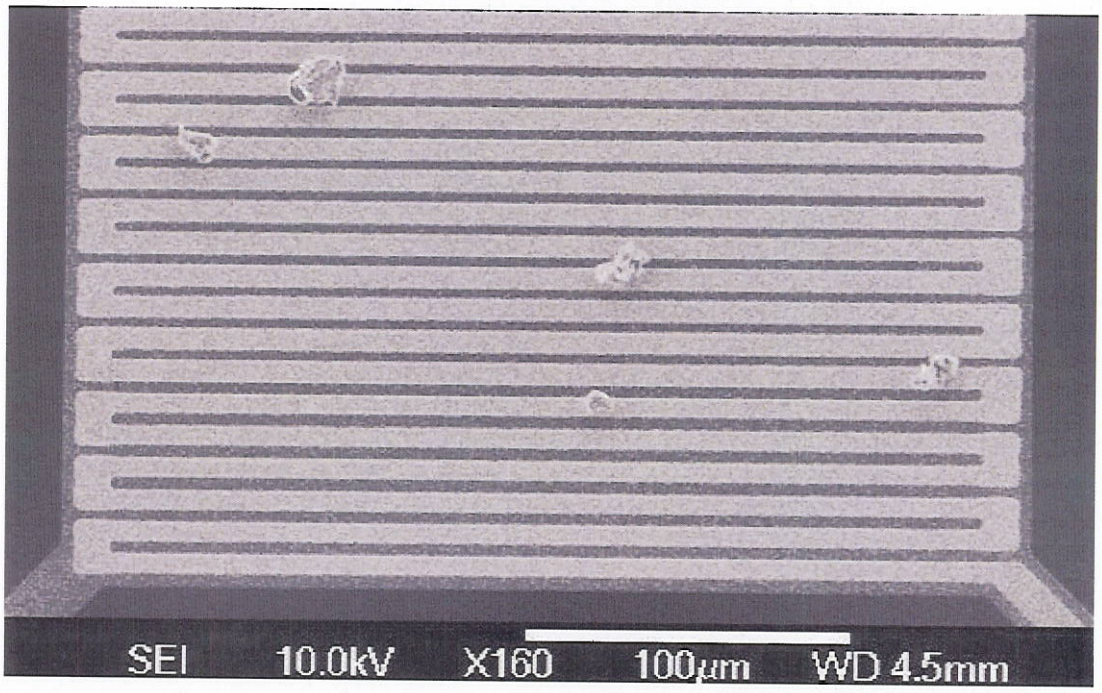

(b) A close-up of the Mg_2SiO_4:Tb,Co microparticles

Figure 28 - Several Mg_2SiO_4:Tb,Co microparticles on a microheater platform, with many more scattered nearby.

Microheaters are used because they are able to rapidly and repeatedly bring the microparticles from room temperature to over 500 °C and back with time constants on the order of tens of milliseconds—32 ms in our current devices, as measured by bolometric methods (Kruse, 1962) — as well as provide a standard linear TL ramp. They are composed of a 200 nm thick etch-released, corner-supported platform of LPCVD silicon nitride topped with a 160 nm Ti/Pt serpentine resistor. The structure designs vary considerably in size but the data reported here use heaters with platforms of side length 300 μm.

The platinum exhibits a highly linear resistance-to-temperature relationship, which is extrapolated by heating the entire device and substrate on a hotplate while measuring the resistance; thereafter, the operating temperature of the microheater can be monitored and controlled via the resistance of the platinum, just as in a common thermistor. Figure 29 shows a set of such measurements for a microheater on the die used here. The microheater is assumed to be at the same temperature as the hotplate surface, measured by a R.T.D. Co. 2823 resistive temperature device located adjacent to the microheater die on the hotplate. Only the temperature range from 35 °C to 60 °C is considered: data below this range are omitted due to insufficiently significant heating, and data above it are excluded because of convection effects. The maximum deviation among the independent linear fits of the data sets when evaluated at 350 °C is 15.57 °C, or 4.4%. The microheater resistance is measured using a Keithley 2410 sourcemeter, which will also serve to drive and monitor the microheater in all pulsed and linear ramp heating reported herein.

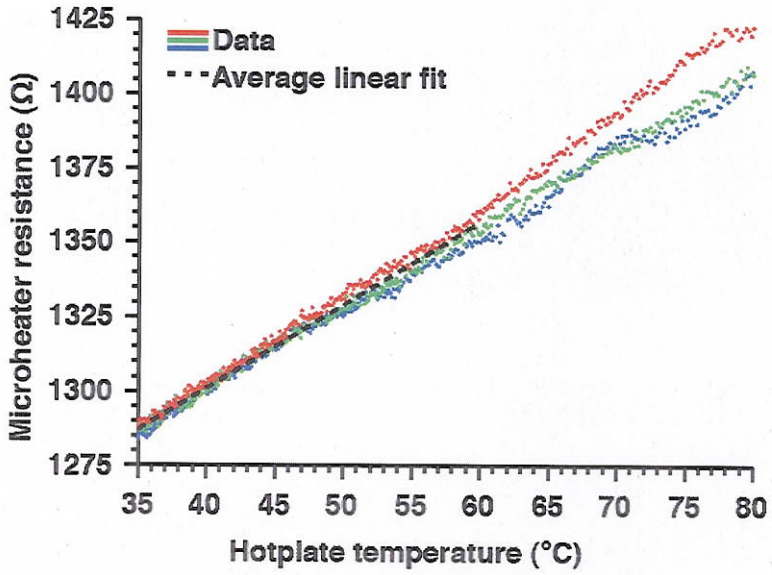

Figure 29 - Three sets of data and the resulting average linear fit for the resistance of a hotplate-heated microheater. Each point represents the average of 5 measurements taken in rapid succession; no other noise reduction has been used. To reduce the effects of inconstant hotplate heating, the measurements are taken as the powered-down hotplate cools to ambient temperature.

Prior to testing, the traps of the microparticles are filled by irradiating with UV light in situ on the microheater by exposure to a broad-spectrum 180–400 nm 30 W deuterium lamp. A 200 ms pulse of variable peak temperature, measured using the platinum thermistor, is administered to a magnesium silicate particle with filled traps. The thermoluminescence glow curve is then gathered using a standard (McKeever, 1985)(Furetta, 2003) linear temperature ramp of 2 °C/sec, reaching to 350 °C. The emitted photons are counted using a Sens-Tech P25PC photomultiplier tube interfaced to a BK 1823A frequency counter. The entire process is automated to run in a room darkened such that the PMT background count is three times its specified maximum dark count. This also eliminates any effects due to photobleaching that are experienced by many, but not all, TL materials (McKeever, 1985). For display, each raw data point is averaged with its 20 closest neighbors (corresponding to approximately 10 °C) and each curve multiplicatively scaled so that their heights are equal at 266 °C, the apex of the second peak. The resulting data evinces a strong background intensity, likely from thermal blackbody emission and nearby TL signatures, which becomes dominant at ramp temperatures above 310 °C after the Mg_2SiO_4:Tb,Co TL peaks have died away. This unwanted signal is modeled as an exponential function curvefitted to the non-pulsed Mg_2SiO_4:Tb,Co above 310 °C, and subtracted from the intensity data of each subsequent pulsed run. The actual TL signatures of interest can then be examined directly. Figure 30 compares the curve-matched background function to the intensity data before and after this background is subtracted.

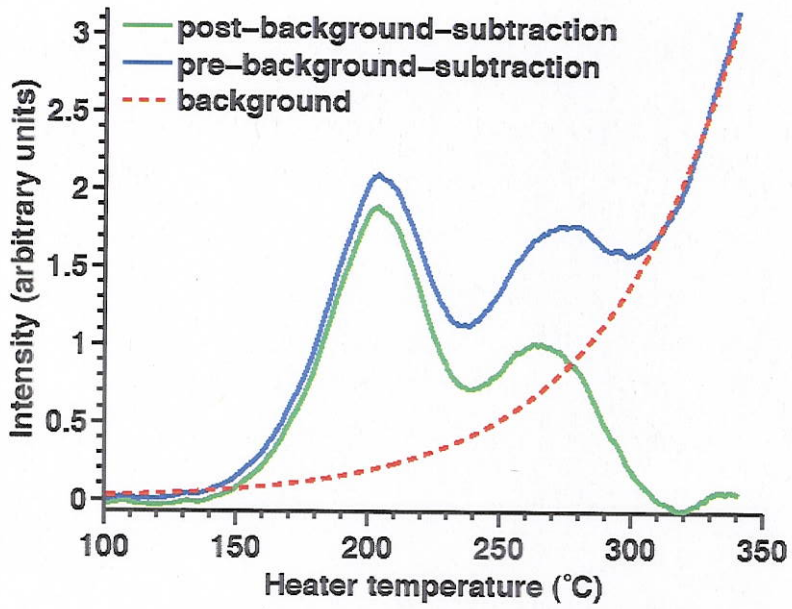

Figure 30 - The intensity observed during the collection of the TL glow curves before and after subtraction of curve-fitted exponential background function.

The resulting thermoluminescence intensity of Mg_2SiO_4:Tb,Co versus linear ramp temperature for a series of different thermal histories, in this case peak pulse temperatures, is shown in Figure 31.

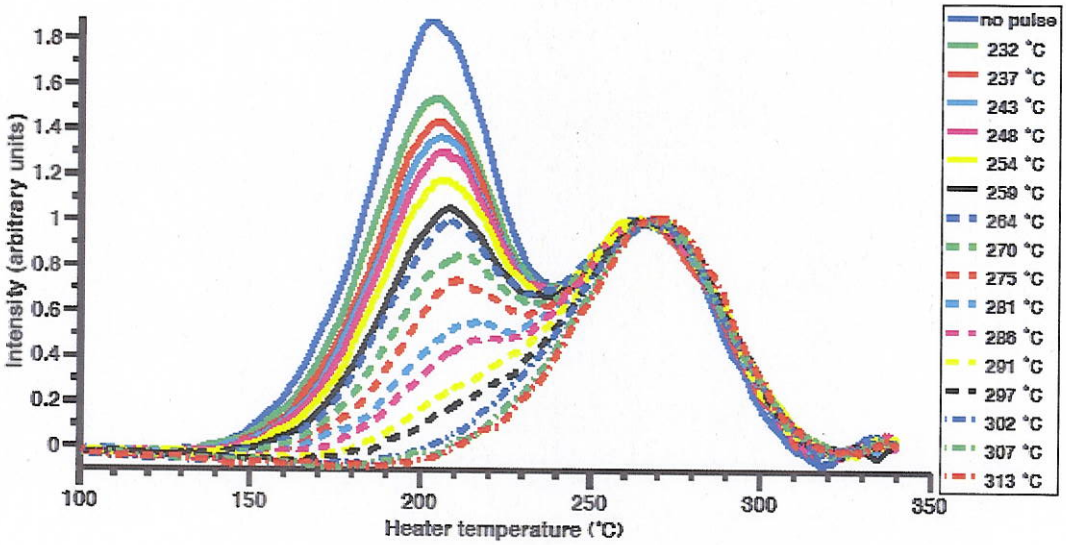

Figure 31 - The thermoluminescence glow curves of Mg_2SiO_4:Tb,Co microparticles after a °190 ms explosive heating pulse. The legend at right indicates the peak temperature of the pulse corresponding to each curve. The intensities shown are normalized at 266 °C, the top of the second observable peak. The ratios of the intensities of the peaks strongly correlate with the maximum temperature to which the particles had been exposed.

4.3.4 Discussion and Theory

The exact mechanics and trap parameters of Mg_2SiO_4:Tb,Co are unknown, and indeed have been observed to vary greatly according to preparation. We therefore modeled the material as two superimposed traps exhibiting first-order kinetics. Under this model, the population n of an electron trap of depth E, frequency factor s, and initial population n_0 after experiencing temperature profile $T(t)$ is given (Randall, 1945) by:

$$n(t) = n_0 \exp\left(-\int_0^t s e^{-E/kT(t)}\, dt\right) \quad (1)$$

If this population value is taken to be n_0' after $T(t)$ has run its course, then the TL intensity observed from the remaining population during a linear temperature ramp $T'(t')$ is expressed as

$$I(t') = C\frac{dn}{dt}$$

$$= n_0'\left(C n_0 \exp\left(-\int_0^t s e^{-E/kT(t)}\, dt\right)\right) s e^{-E/kT'(t')} \quad (2)$$

where C is a constant. Lacking knowledge of the trap parameters of this material, we chose E, s, and n_0 values that best fit our non-pulsed experimental curve; numerical simulations based on the preceding equations were then used to produce pulsed glow curves for these theoretical particles. Figure 32 compares the relation between the intensity peak height and temperature pulse maxima of the resulting simulations to that of the experimental data seen in Figure 31.

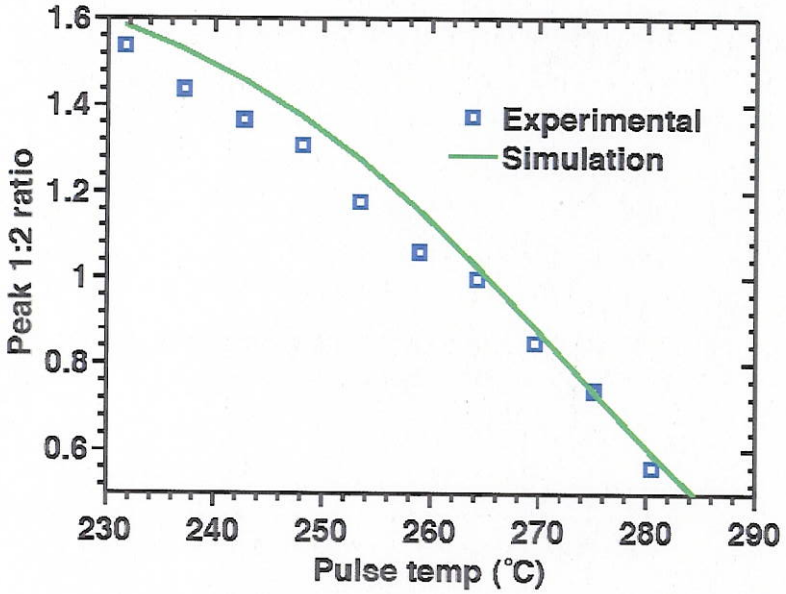

Figure 32 - The ratio of the height of the first TL peak to the height of the second as a function of pulse temperature for simulated and experimental data.

A one-to-one decrease occurs in the intensity ratio of the first peak to second peak heights as the pulse temperature climbs. The slope of the curve is reasonably stable, indicating that the sensitivity of the material will be fairly steady over the usable pulse temperature range. In the range we observed, model and data differed by an average of 4.4%, with no errors greater than 9.1%. It is therefore possible to deduce the pulse temperature from the TL glow curve by comparing the ratios of intensity peak heights, provided the length of the pulse is known. Even better accuracy would be obtained by simply curve fitting the TL peak ratio in much the same manner that the resistance of commercial thermistors is calibrated. With this particular material and temperature pulse duration the first TL peak becomes indistinguishable after the pulse temperature passes 290 °C, but other TL materials with deeper traps could be substituted or used in parallel to take over from Mg_2SiO_4:Tb,Co at this point.

To conclude this section, we have demonstrated the recovery to good accuracy of the peak temperatures, ranging from 232 °C to 313 °C, experienced in a microheater-powered rapid heating event of known duration less than 200 ms. The observed change in the thermoluminescence peak intensity ratio of two Mg_2SiO_4:Tb,Co traps has been predicted with an average error of 4.4% using first-order kinetics modeling.

4.4 Characterization of existing dosimetric materials for thermometry

4.4.1 Overview of the material research and literature research

In spite of the relatively large availability of TL materials for dosimetry application, most of the materials available are not suitable for temperature sensing. This stems from the fact that the requirements for dosimetry are different than the requirements for temperature sensing. Detectors that would be ideal for temperature sensing were usually rejected as dosimetric materials in the past.

The characteristics of materials of interest for temperature sensing are the following:

(i) High thermoluminescence output (*i.e.*, high sensitivity);
(ii) Presence of several thermoluminescent peaks covering a wide range of temperatures;
(iii) First-order kinetic behavior or thermoluminescence;
(iv) Thermal stability of the thermoluminescent peaks;
(v) Optical stability of the thermoluminescent peaks (*i.e.*, TL is insensitive to light);
(vi) Chemical and mechanical stabilility.

There is currently no material satisfying all the criteria above and, therefore, research into new luminescent materials that may have been previously ignored for dosimetry applications is of paramount importance.

The material investigations in this project focused on silicates and oxides due to their chemical stability. They included new nanophosphors produced by Luiz B. Jacobsohn and Michael Blair at Los Alamos National Laboratory (LANL), and natural materials known to exhibit potentially good thermoluminescence properties (natural topaz). The main findings are described below.

4.4.2 Commercial dosimetric materials

4.4.2.1 Al_2O_3:C

Al_2O_3:C is one of the most sensitive TL and OSL material available with relatively well-known TL properties (McKeever et al., 1995). Furthermore, its hardness and resistance to chemical attack makes this material ideal for harsh environments. The problem is that the TL of Al_2O_3:C is dominated by a peak at 180°C, which is the peak used in dosimetry. Therefore, to extend the application of the material to higher temperatures, it is necessary to investigate its high-temperature peaks.

Figure 33 shows the TL curves of Al_2O_3:C after irradiation with a high dose of 300 Gy and pre-heating to 280°C to eliminate the main dosimetric peak. The residual TL curve shows various peaks ranging from 300°C to 600°C which can be useful for thermal sensing.

The problem of using TL of Al_2O_3:C is that the thermal quenching, *i.e.*, reduction in luminescence efficiency with increasing temperatures, decreases the intensity of the TL peaks significantly. The solution to this problem is to try using optical stimulation to access these deep traps, taking advantage of the fact that OSL is measured at room temperature and, therefore, it is not affected by thermal quenching.

The possibility of probing the deep traps associated with the high-temperature TL peaks in Al_2O_3:C was investigated using blue light. Figure 34 shows the effect of illumination on the TL peaks. It is clear from this data that blue stimulation can effectively deplete the charge carriers in these deep traps and, therefore, can be used to probe the signal and obtain a calibration curve similar to the one shown in Figure 43b, but for the OSL signal instead of TL signal.

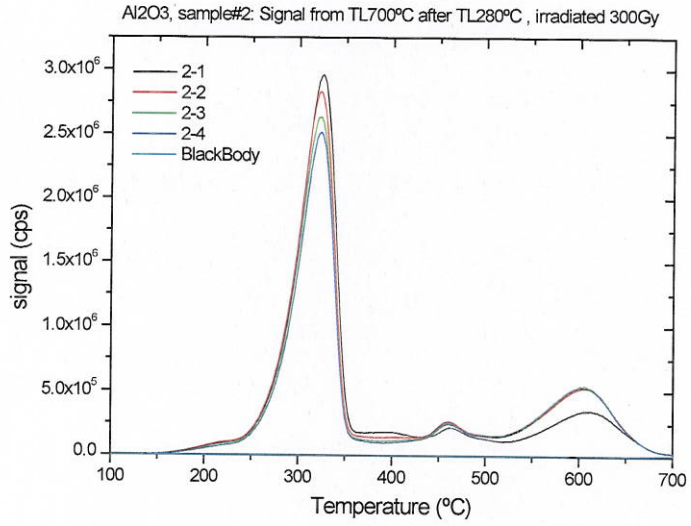

Figure 33. Al_2O_3:C sample irradiated with 300 Gy, and pre-heated to 280°C to remove the main dosimetric trap at 180°C, revealing the deep traps present in the material.

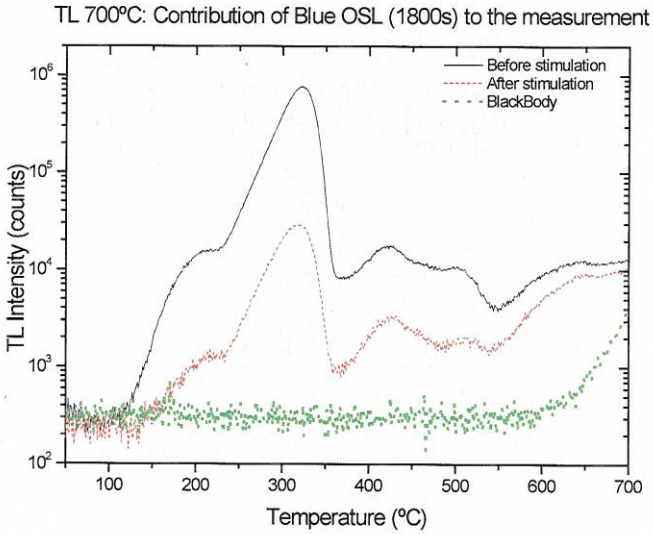

Figure 34. Effect of blue stimulation on deep traps of an Al_2O_3:C single crystal. The sample was irradiated with 300 Gy and pre-heated to 280°C to remove the main dosimetric trap. The graph shows the remaining TL curve before and after blue stimulation for 1800 s (LEDs centered at 470 nm, ~50 mW/cm^2).

4.4.2.2 LiF:Mg,Ti

LiF:Mg,Ti is a TL material widely used in TL dosimetry (McKeever et al., 1995). However, there are several properties that make this material of interest for temperature sensing, including the presence of several TL peaks, the thermal stability, the insensitivity to light exposure, and the ready commercial availability. The disadvantage is the complex defects associated with the TL process, which may affected our ability to extract information from the TL curves. Here we present some of the tests performed with this material for application in temperature sensing. More detailed investigations were carried out using this material in Section 4.4.2.

Figure 35 shows that the TL curves of LiF:Mg,Ti are very reproducible, which is a requirement for use of the material as a temperature sensor. The material also shows high sensitivity. The TL intensity of ~10 grains reaches an intensity close to saturation of the PMT (Figure 36). The TL peaks above 100°C are stable at room temperature and could be used as temperature sensors (Figure 37).

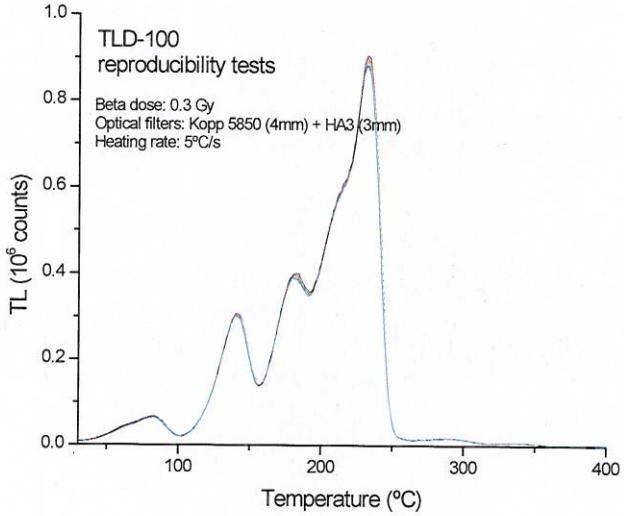

Figure 35. Reproducibility test of LiF:Mg,Ti. The data shows the TL curves for five cycles of irradiation and TL readout. The results demonstrate the reproducibility of the TL curves from this material.

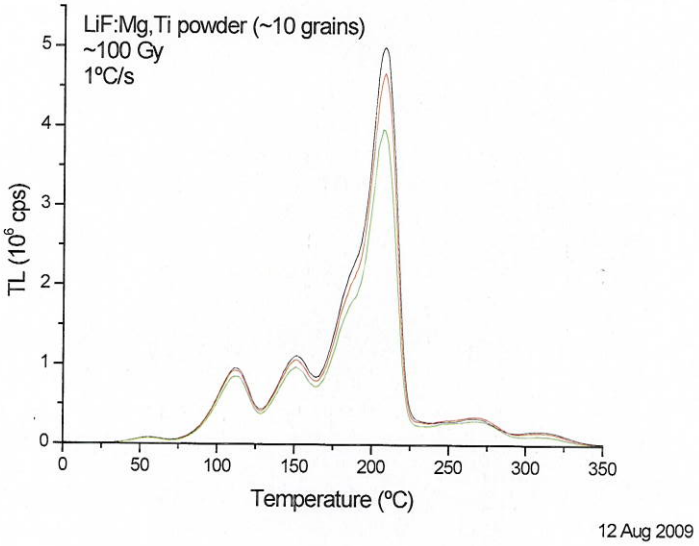

Figure 36. TL curves of grains of LiF:Mg,Ti irradiated with a large dose. This curves provide an idea of the TL intensity that could be obtained for single grains of the material to be used in temperature sensing. The signal intensity (~10^6 cps) is close to the saturation of the PMT.

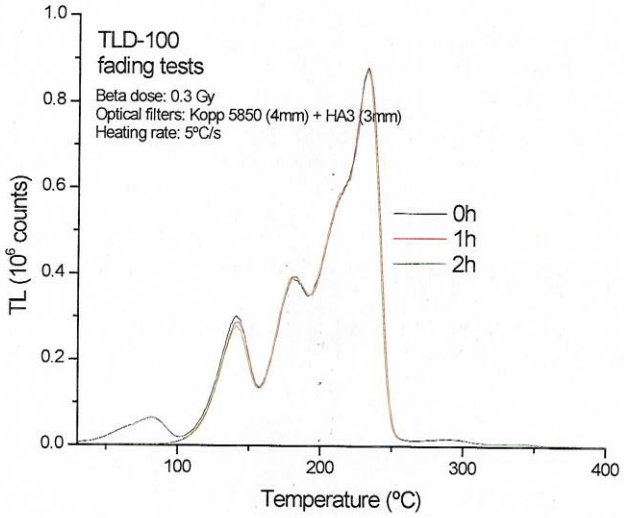

Figure 37. TL curves of LiF:Mg,Ti immediately following irradiation and after 1 or 2 h after irradiation. The data demonstrates that the TL peaks at temperatures higher than 100°C are relatively stable and could be used to temperature sensing. The peaks below 100°C decay at room temperature and are not suitable for temperature sensing.

4.4.3 Materials under development

4.4.3.1 Silicates and aluminates

Most of the TL materials available today were developed for radiation dosimetry applications and optimized to have a single or easily distinguished TL peak. On the other hand, for the applications intended in this project new materials with multiple, equally intense TL peaks are necessary. Therefore, it is necessary to research new materials that could be used as "model" materials to test our hypothesis and eventually for the real application in temperature sensing.

Figure 38 shows the TL curves of several silicates and aluminates that we obtained through other collaborations and investigated for potential application as temperature sensors. The materials have very different distribution of trapping centers, but the Mg_2SiO_4 samples (Figure 38b) shows an interesting combination of high intensity TL peaks. Sample 16 is particularly interesting due to the presence of at least three TL peaks in the range from 150°C to 400°C.

The reproducibility of the TL curves from Mg_2SiO_4:Tb,Co (sample 16) is demonstrated in Figure 39, which shows the TL curves obtained after five cycles of readout and irradiation. The intensity of the TL curves do not deviate by more than 2%.

Figure 40 demonstrates the thermal stability of the TL peaks under normal conditions of storage at room temperature. Except for the low temperature portion of the TL curve <100°C, the TL peaks are relatively stable over up to 24 h of storage.

Figure 41 shows the TL curves of Mg_2SiO_4 sample 16 as a function of maximum temperature of the pre-heating. The behavior of the TL peaks is similar to the model predictions, showing decrease of the TL peaks at different temperatures (see Figure 3). If the TL peak intensity is

plotted against the maximum pre-heating temperature, the graph shown in Figure 42 is obtained. This graph allows one to determine the maximum temperature reached by the crystal in laboratory conditions.

The procedure for determining the maximum temperature is illustrated in Figure 43. Suppose that a material irradiated with a known dose is heated to an unknown temperature and, after recovery, the TL curve is measured (dashed line). The material can then be irradiated again with the same dose to record the original TL curve (solid line). Comparison between these two curves (Figure 43a) together with the calibration curve obtained in laboratory (Figure 43b) allows the maximum temperature to be determined.

This simple approach illustrates the usefulness of the technique, but more advanced mathematical procedure such as glow curve deconvolution.

In this particular case, the calibration curve is valid only for the heating rate used in the experiments. However, as shown in the simulations, the variation in the calibration curve decreases as the heating rate increases. The calibration curve can then be obtained for fast heating rates and realistic time-temperature profiles using the microheaters developed in the present project.

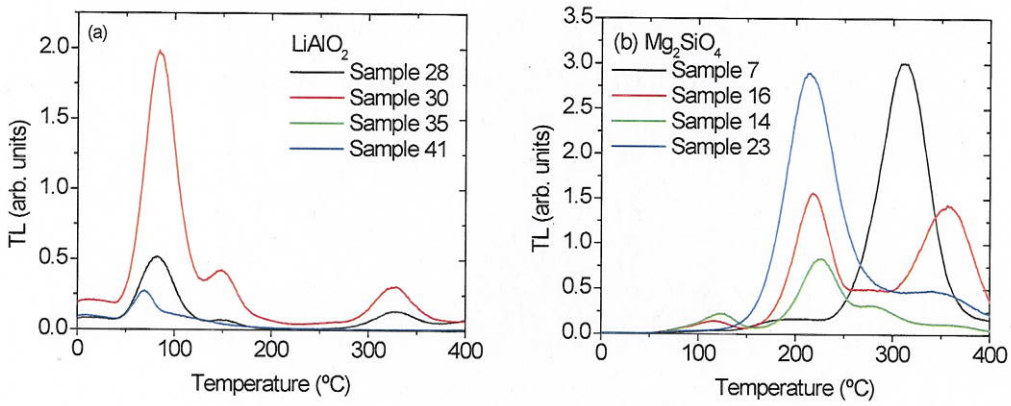

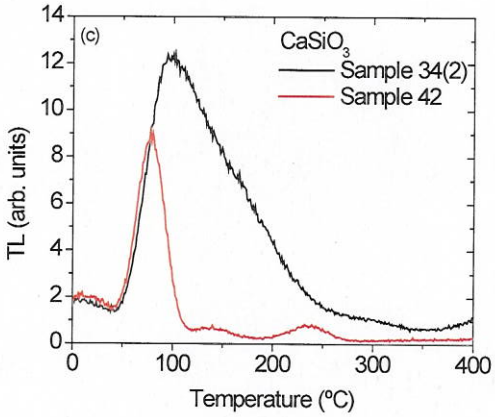

Figure 38. TL curves of 10 different new TL/OSL materials. The multiple TL peaks in the Mg_gSiO_4 samples makes them a suitable materials for testing.

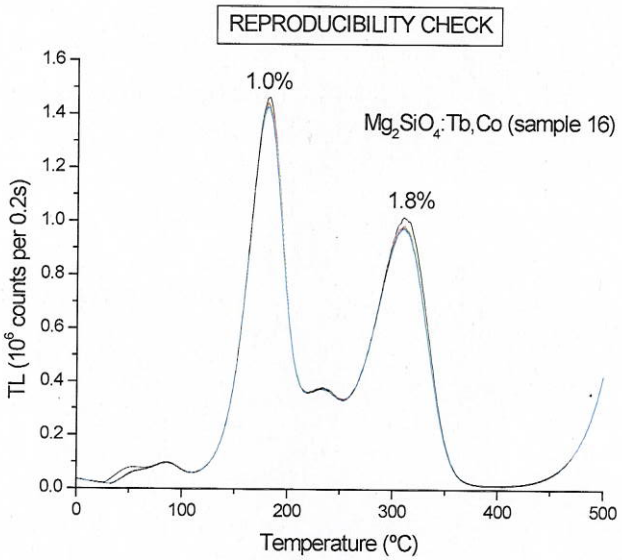

Figure 39. Reproducibility of the TL curves from Mg_2SiO_4:Tb,Co (sample 16) after five cycles of readout and irradiation with the same dose.

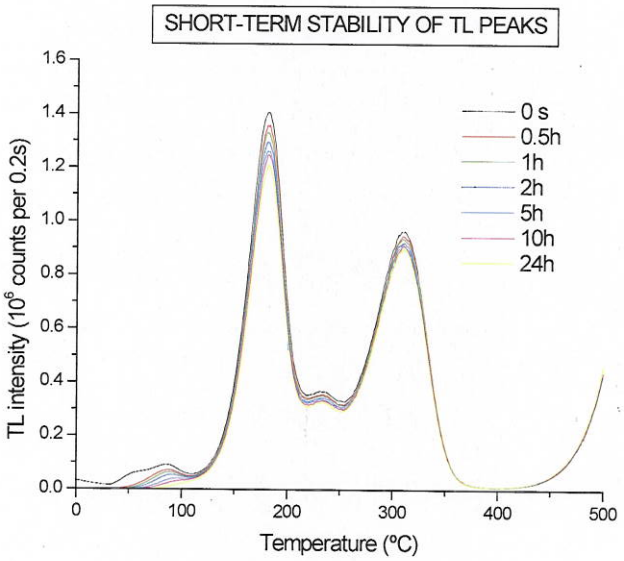

Figure 40. Short term stability of the TL peaks from sample Mg_2SiO_4:Tb,Co (sample 16). The sample was irradiated and TL readout was performed after various interval of time following irradiation.

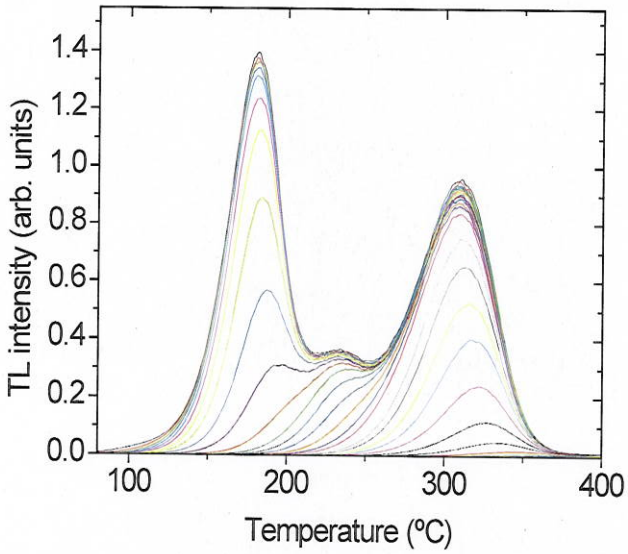

Figure 41. TL curves of $MgSiO_4$ samples after irradiation with 300 Gy and pre-heating to increasing maximum temperatures T_{max}. Each curve corresponds to a specific maximum temperature T_{max}.

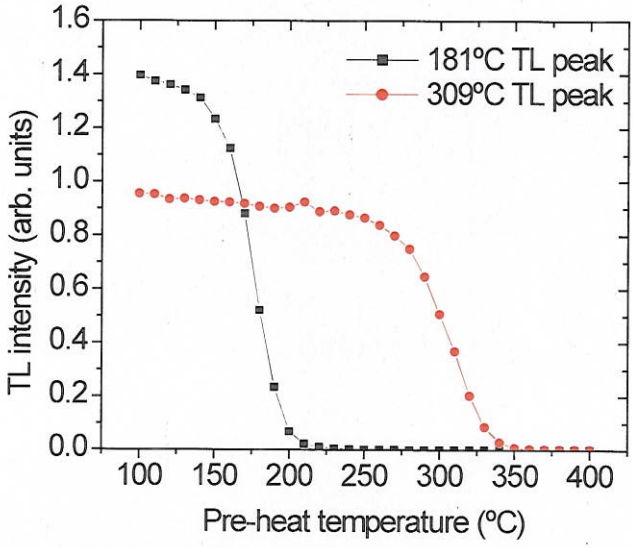

Figure 42. Intensity of the two prominent TL peaks in $MgSiO_4$ as a function of maximum pre-heating temperature.

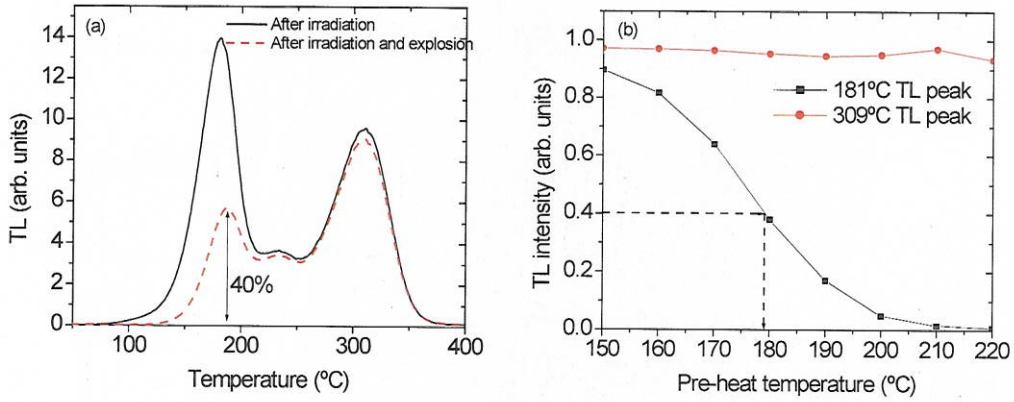

Figure 43. Illustration of one approach to determine the maximum temperature experienced by the luminescence material.

4.4.3.2 Oxyorthosilicates (YSO, GSO, LSO)

A comparison was made between powder obtained from materials produced by single crystal growth (Czochraslki method) and nanophosphors produced by Solution Combustion Synthesis (SCS). Table 4 summarizes some of the characteristics of the samples, where the most important result is the radioluminescence (RL) intensity. This measurement demonstrates that the intensity

of the radioluminescence of the nanophosphors is comparable to oxyorthosilicates produced by single crystal growth, indicating that the Solution Combustion Synthesis can successfully produce materials of comparable light yield for scintillation applications.

Figure 44 shows the thermoluminescence curves of the various samples, normalized to the mass of material used in the measurements. The curves show first-order behavior, as indicated by the fact that the curve shape is independent on the dose (see insets in Figure 44). However, the thermoluminescence intensity of the nanophosphors is relatively low compared to the bulk crystals. This indicates a low concentration of trapping centers.

Another disadvantage is the lack of thermal stability of the TL curves. Figure 45 shows the TL curves for various samples for different times after irradiation. Except for the YSO produced by Czochralski method, all samples show a significant fading even in the high temperature regions of the TL curve (see Figure 45b).

The oxyorthosilicate samples also exhibit strong sensitivity to light, as shown in Figure 46. Light exposure eliminates most of the TL signal induced by radiation. This characteristic hampers the use of these materials in experiments where light exposure cannot be avoided.

In summary, oxyorthosilicate nanophosphors have shown to have excellent properties for use as scintillating materials in radiation detection, but their usefulness for temperature sensing seems to be limited by the low concentration of trapping centers, strong fading of the signal, and light sensitivity. However, we should not exclude the possibility of finding other nanophosphors that do not show the properties above.

Table 4. Main properties and characteristics of bulk and nanophosphor samples of LSO, GSO, and YSO used in this study.

Property/detail	*LSO (bulk)*	*SCS-LSO-24*	*GSO (bulk)*	*SCS-GSO-8*	*YSO (bulk)*	*SCS-YSO-26*
Synthesis	Czochralski	SCS	Czochralski	SCS	Czochralski	SCS
Grain size range	125-250 μm	20-100nm	75-125 μm	20-100nm	45 μm	20-100nm
RL intensity (10^3 counts s^{-1} mg^{-1})[(a)]	49.0 ± 2.4	64 ± 4	94 ± 13	36 ± 4	97 ± 14	44.3 ± 1.5
Main TL peaks[(b)]	340 K (I) 405 K (II) 480 K (III) 565 K (IV)	345 K	373 K	365 K	398 K	365 K
E (eV)[(c)]	1.129	0.782	1.016	1.009	1.005	0.987
s (s^{-1})[(d)]	1.73×10^{15}	2.07×10^{10}	4.42×10^{12}	8.14×10^{12}	3.83×10^{11}	3.58×10^{12}

[(a)] Radioluminescence measured under X-ray excitation (35 kV_p) using Schott BG-39 filters in front of the PMT. The values are the mean and experimental standard deviation of the values obtained for three aliquots with weight between 1.5 and 10 mg.
[(b)] Based on TL curves measured at 1°C/s.
[(c)] Activation energy for peak I determined using the Initial Rise Method.
[(d)] Frequency factor for peak I calculated based on the activation energy and temperature of the peak, assuming a first-order TL process.

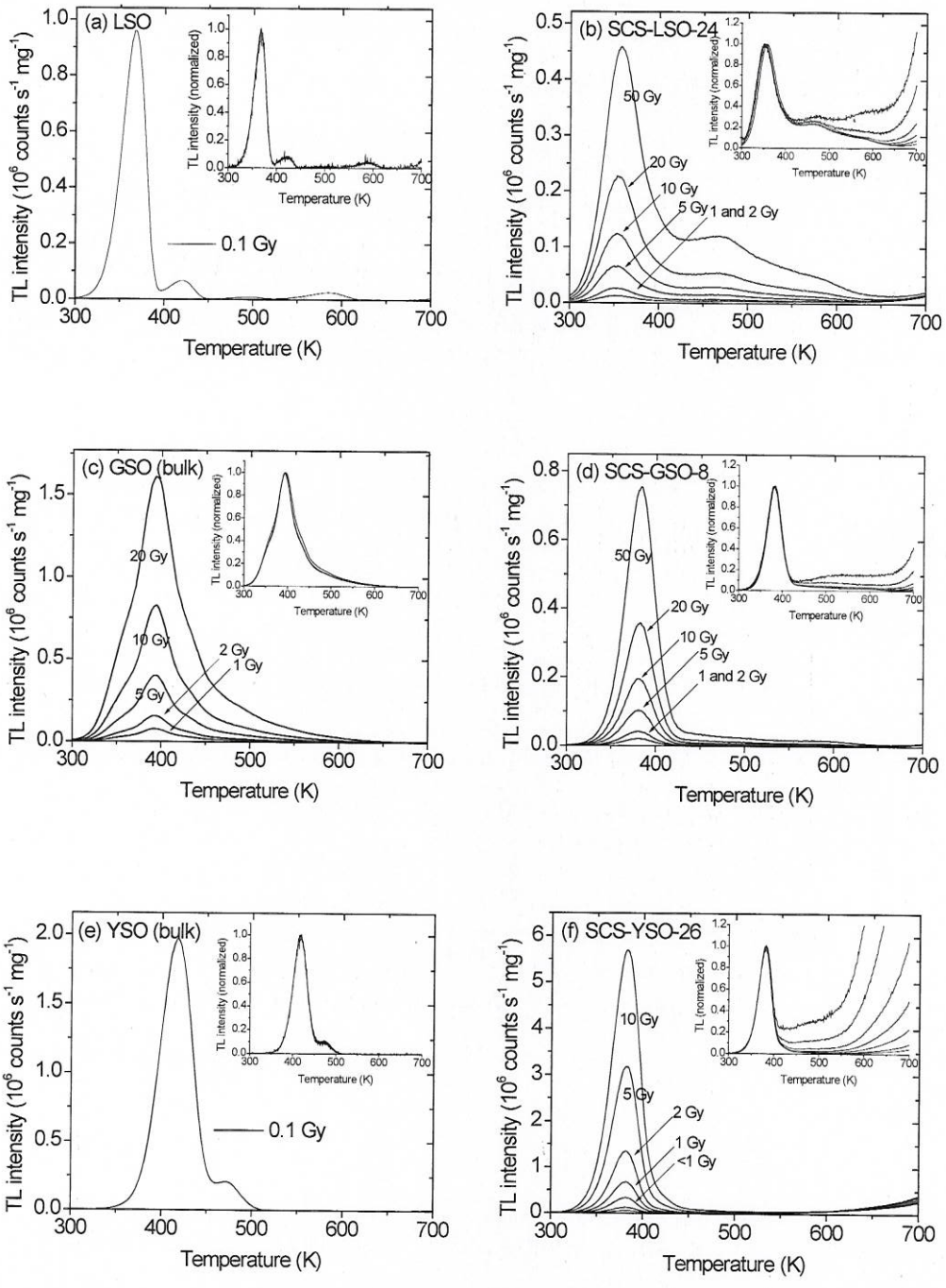

Figure 44. TL curves of oxyorthosilicates produced by the Czochralski method as compared to oxyorthosilicates produced by the Solution Combustion Synthesis (SCS) method. (See text for more details.)

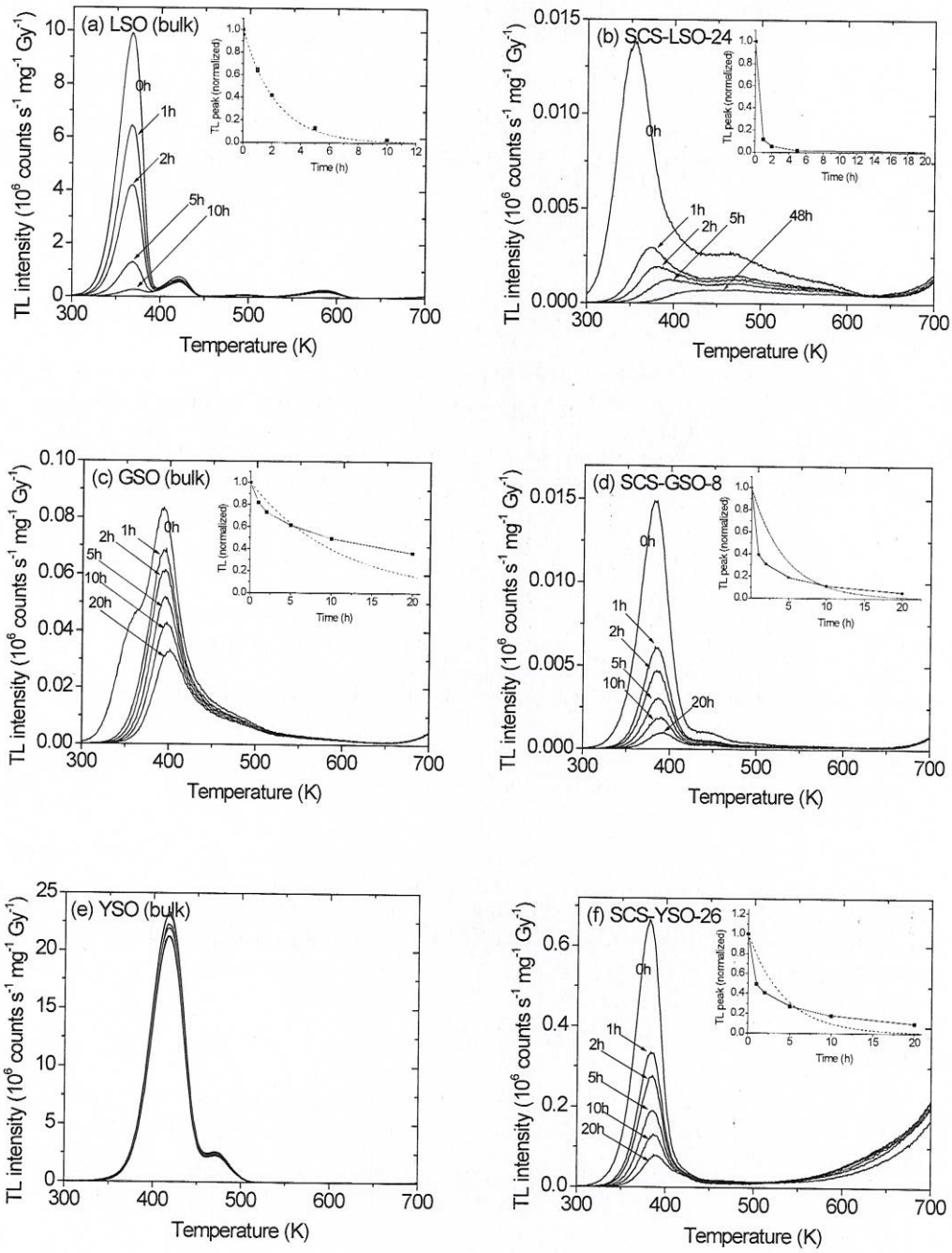

Figure 45. TL curves of oxyorthosilicates produced by the Czochralski method and nanophosphors produced by the Solution Combustion Synthesis (SCS) method for various intervals between irradiation and measurement.

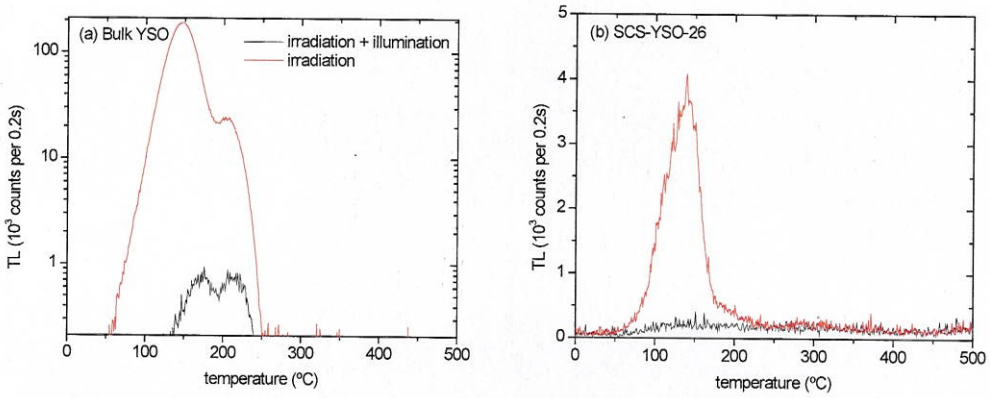

Figure 46. Light sensitivity (blue LED illumination) of YSO oxyorthosilicate samples prepared by (a) Czochralski method and (b) Solution Combustion Synthesis method.

4.4.4 Natural materials

An alternative route to finding materials with suitable properties for this project is to investigate natural crystals. The advantage is that natural crystals have a variety of trapping centers and, whereas the concentration and type of defects may vary, properties associated with the matrix may indicate the type of materials that could be produced in the future. Natural topaz, $Al_2SiO_4(F,OH)_2$, is a material that has been investigated for radiation dosimetry and is known to have TL emission (Yukihara and Okuno, 1998).

The samples used in this study are two natural samples from Brazil, labeled JMI01 and JOZ07. The TL curves of these samples are shown in Figure 47, where one can see one excellent characteristic for temperature sensing: the presence of several TL peaks in a temperature range from room temperature up to 500°C. The TL curves exhibited good reproducibility, as shown in Figure 48. The TL curves grow with dose (Figure 49) and the curve shape depends only slightly on the irradiation dose (Figure 50), except for the high temperature region which is affected by the background emission due to blackbody radiation. This indicates that the curves can be described by a superposition of first-order TL peaks, as required in this project.

The low temperature TL peaks are naturally unstable at room temperature, but Figure 51 shows that the high temperature peaks are not affected by blue light. So, as opposed to all materials previously investigated, topaz seems to be light insensitive. In addition, Figure 52 shows that TL can also be induced by UV illumination, although in this case the TL curve is significantly different from the beta induced TL curves. More investigations need to be performed to determine whether UV can be used or not to fill the traps in the intended application.

The only drawback observed so far is the low light intensity of the TL from natural topaz. Table 5 compares the TL light yield from topaz as compared to Al_2O_3:C, where one can see that topaz

is at least three orders of magnitude less bright than Al_2O_3:C. Nevertheless, it should be pointed out that this is not surprising, since Al_2O_3:C is one of the most sensitive luminescent dosimeters available today. As long as one can measure sufficient TL signal from the grains to be used in the temperature measurements, the overall sensitivity should not be a problem.

In spite of the low TL intensity, the natural topaz samples have shown good properties to serve as a test materials: reproducibility, almost first-order behavior, and light insensitivity. We intend to perform tests for the intended application using this sample, at least until a more suitable material is found or produced.

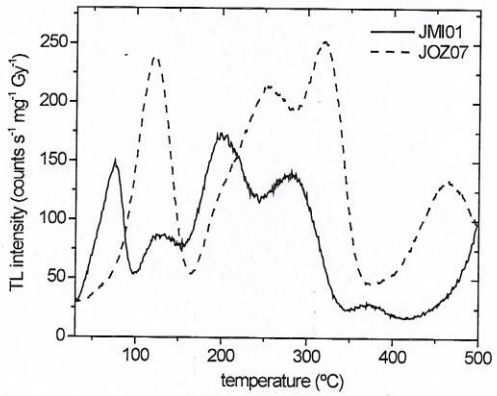

Figure 47. TL curves of two topaz crystal samples, JMI01 (single crystal, 28mg) and JOZ07 (powder, 20mg). The TL measurements were carried out at 1°C/s using Kopp 5850 + HA3 optical filters in front of the PMT. The samples were irradiated with beta rays from a $^{90}Sr/^{90}Y$ source. The TL intensities were normalized to the mass of the sample and dose of radiation.

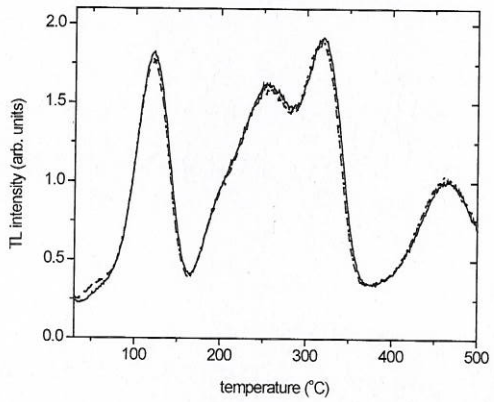

Figure 48. TL curves of topaz sample JMI01 (single crystal, 28 mg) repeatedly irradiated with 3 Gy. The TL measurements were carried out at 1°C/s using Kopp 5850 + HA3 optical filters in front of the PMT.

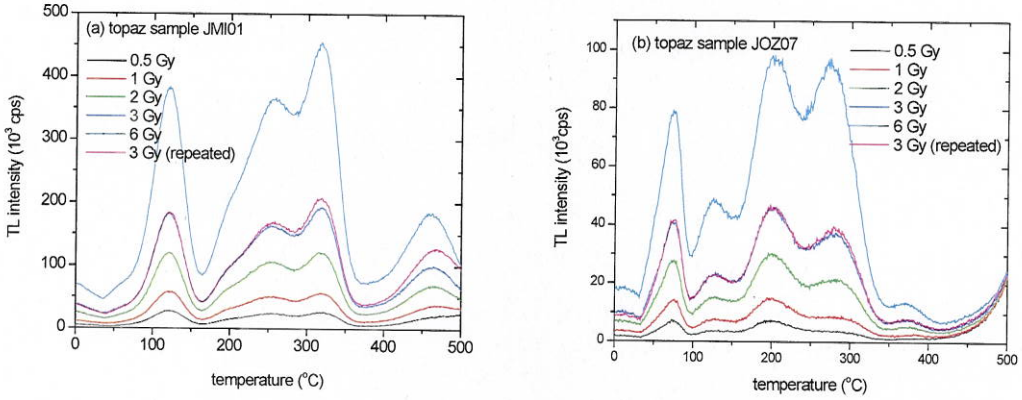

Figure 49. TL curves of topaz sample JMI01 (single crystal, 28 mg) and JOZ07 (powder, 20 mg) for various irradiation doses up to 6 Gy. The TL measurements were carried out at 1°C/s using Kopp 5850 + HA3 optical filters in front of the PMT.

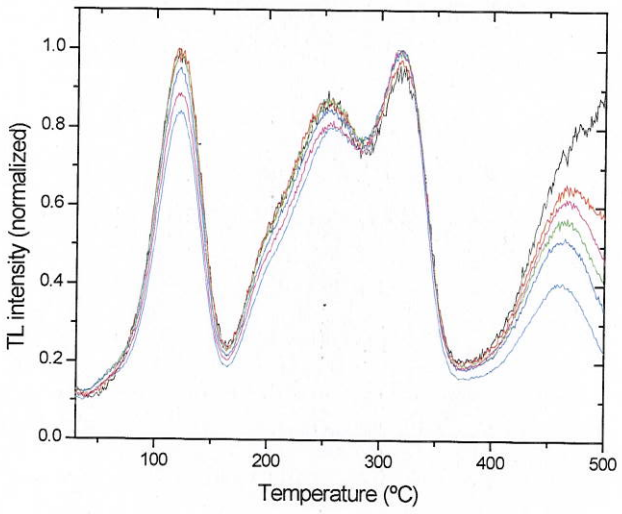

Figure 50. Normalized TL curves of sample JMI01 (single crystal, 28 mg) irradiated with various doses (data shown in Figure 49a).

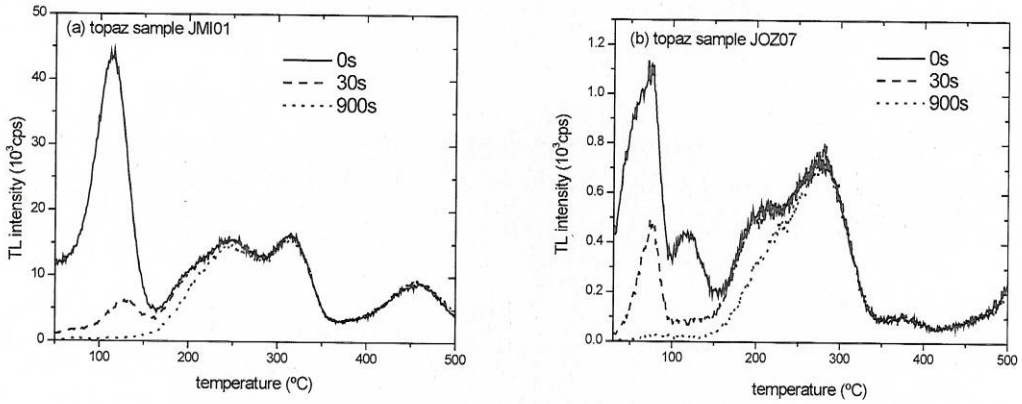

Figure 51. TL curve of irradiated topaz samples JMI01 (single crystal, 28 mg) and JOZ07 (powder, 20 mg) as a function of blue illumination time. The samples were irradiated with 3 Gy of beta rays from a $^{90}Sr/^{90}Y$ source and illuminated with blue light from LEDs (470nm, 20 mW/cm^2). TL measurements were carried out at 1°C/s using Hoya U-340 optical filters in front of the PMT.

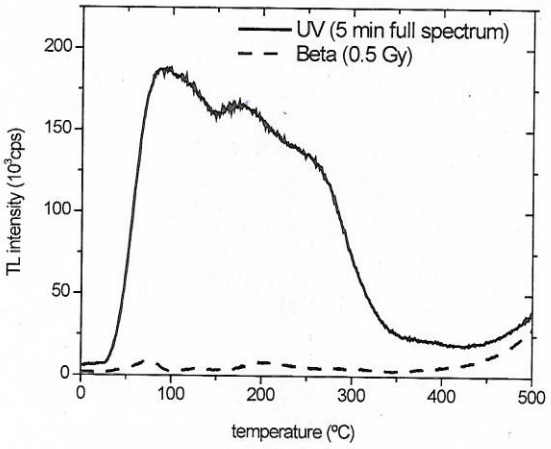

Figure 52. TL curves of topaz sample JOZ07 (powder, 20 mg) after UV illumination and beta irradiation. The UV illumination consisted in exposure to unfiltered light from a deuterium lamp (2.44 mW/cm^2 at the sample position) for 5 min, and the beta irradiation dose was done using a $^{90}Sr/^{90}Y$ source. The TL measurements were carried out at 1°C/s using Kopp 5850 + HA3 optical filters in front of the PMT.

Table 5. Light yield comparison between topaz samples and dosimetric Al_2O_3:C. The samples

Material/Sample	*TL yield (counts mg^{-1} mGy^{-1})*	*Relative TL yield (%)*
Al_2O_3:C	1920	100
Topaz/JMI01	2.57	0.13
Topaz/JOZ07	1.37	0.07

4.4.4.1 Kyanite, sillimanite, and andulusite

Kyanite, sillimanite, and andalusite are polymorphs of aluminum silicate (Al_2SiO_5). They were investigated here to explore the TL properties of this type of material. Unfortunately, these materials showed only low temperature TL peak (<100°C) which is not suitable for temperature sensing.

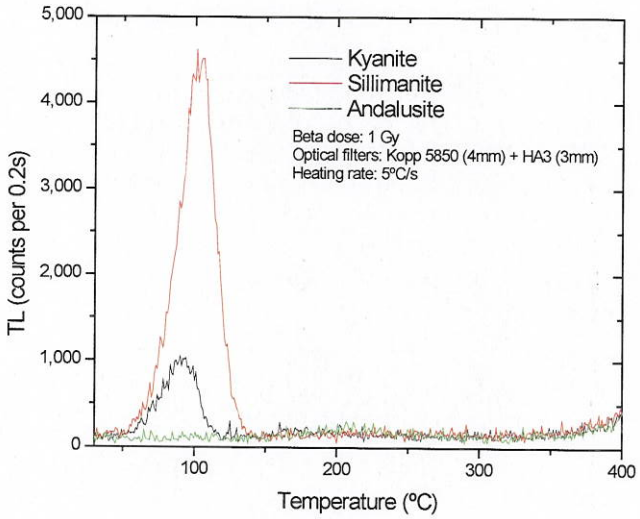

Figure 53. TL curves of kyanite, sillimanite, and andalusite, which are natural forms of Al_2SiO_5, after irradiation with 1 Gy.

4.5 Development of new materials for luminescence thermometry

4.5.1 Solution Combustion Synthesis

In this project we became interested in the possibility of developing new TL materials for temperature sensing using the SCS method (see Section 3.2). Attractive points of this technique include:

- Simplicity and cost-effectiveness;
- High yield (mass content);
- Capability to achieve high purity crystalline materials;
- Capability to synthesize multiphase complex oxide powders.

We focused on demonstrating that the SCS method has the potential to produce materials with high TL intensity and various TL peaks that could be useful for thermometry. The goal is to identify potential materials and understand how to control the synthesis conditions to engineer the materials with the desired properties.

Figure 54 shows examples of X-ray diffractograms of materials synthesized using the SCS technique, demonstrating the possibility of obtaining crystalline samples.

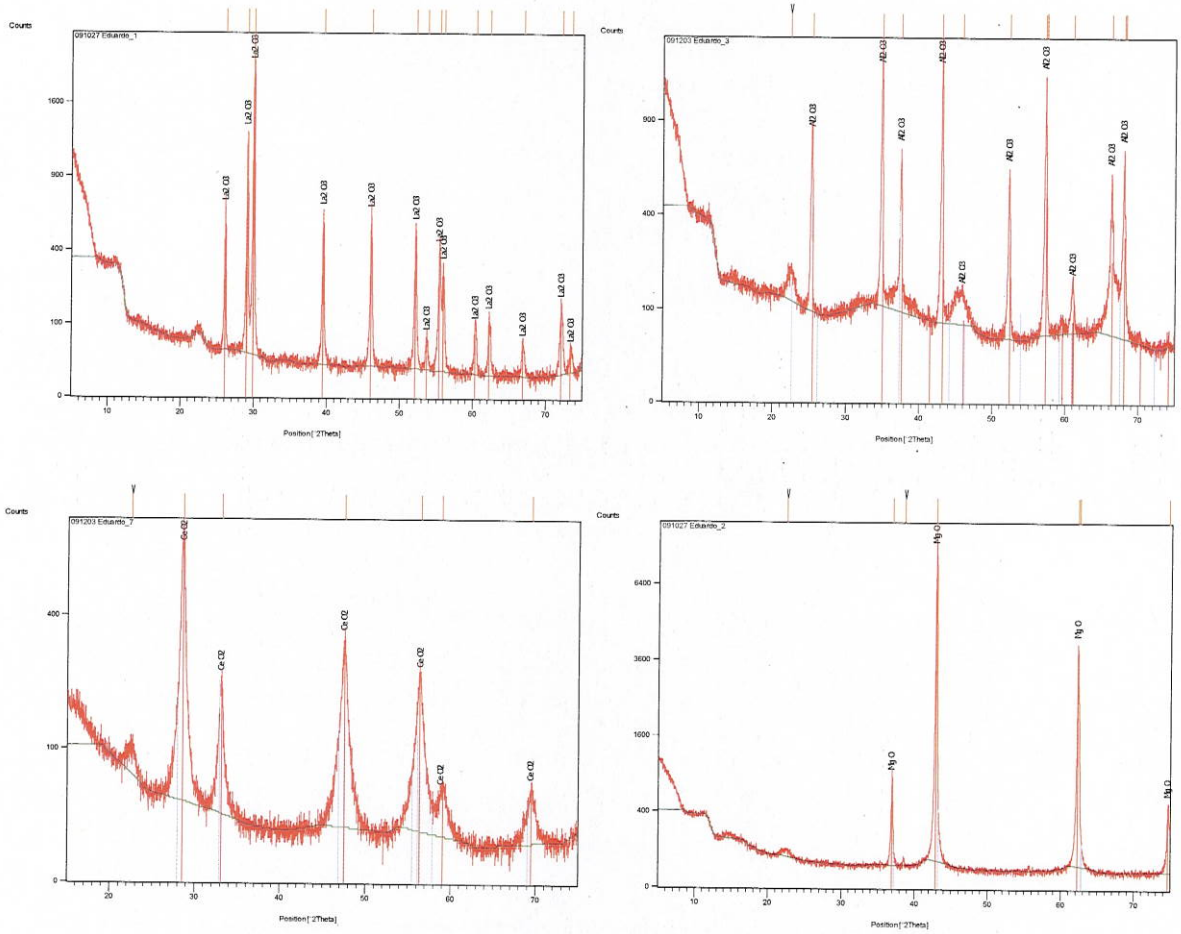

Figure 54. XRD for four different materials produced by SCS: La_2O_3, Al_2O_3, CeO_2, and MgO.

4.5.1.1 Luminescence from SCS samples

As discussed in Section 3.2, several compounds were synthesized as part of this investigation. Figure 55 shows examples of a variety of ceramic materials prepared by SCS. The results reveal a variety of TL curves which increase with the dose of ionizing radiation, as desirable in a TL material. In these examples, the TL intensity is usually not very high, but at this point the experimental parameters for synthesizing these materials had not been optimized.

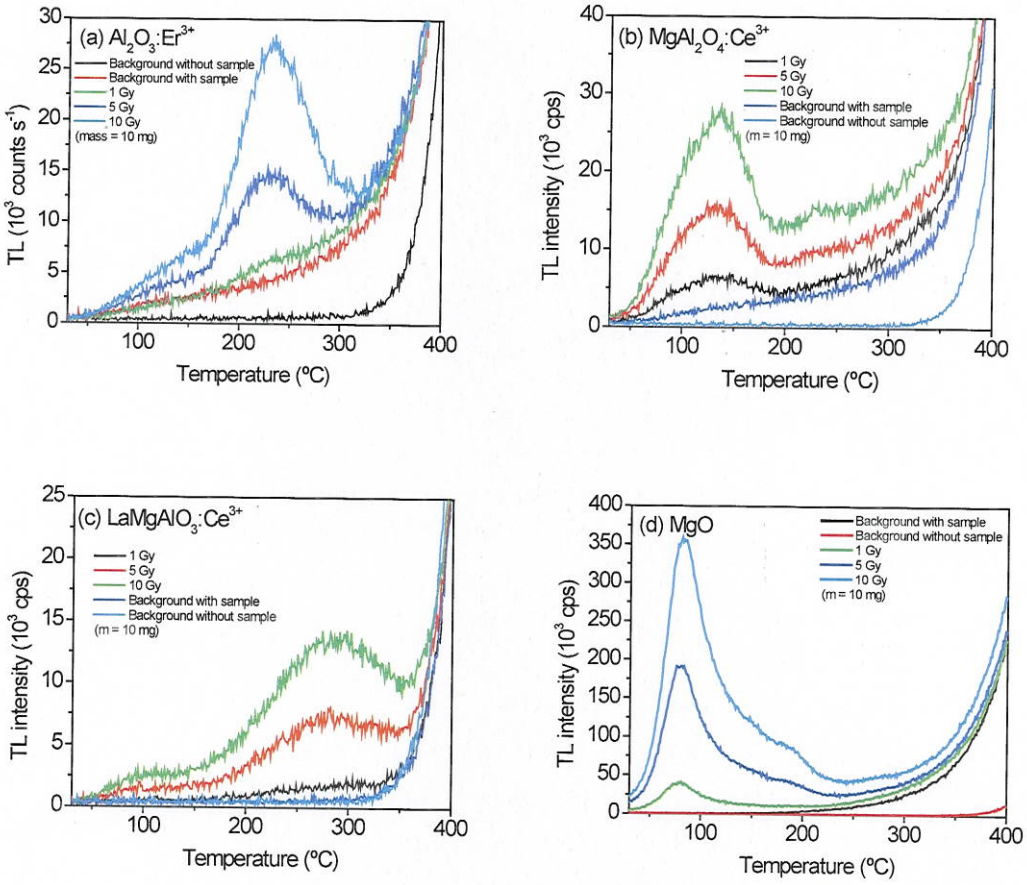

Figure 55. TL glow curves obtained after beta irradiation of (a) $Al_2O_3:Er^{3+}$, (b) $MgAl_2O_4:Ce^{3+}$, (c) $LaMgAlO_3:Ce^{3+}$, and (d) MgO. All samples were prepared by SCS and annealed at 900 °C during 2 h in air.

An important part in engineering new materials is to introduce luminescence centers with emission that matches the detection systems used for TL readout. To investigate if appropriate doping can be used with the SCS technique to control the luminescence centers, we synthesized MgO doped with different dopants and measured the RL emission spectrum (Figure 56). A tentative assignment of the emission bands in the RL spectrum observed in MgO doped with different dopants is also depicted. The emission band in the Ce^{3+}-doped MgO is attributed to the $5d^14f^0 \rightarrow 4f^1$ transition of Ce^{3+} ion, in agreement with the one reported by Bapat and Sivaraman {, 1986 #683} in $MgO:Ce^{3+},Li^+$. Emission from Ce^{3+} is known to vary from blue to the red region of the spectrum, depending on the crystal field (Blasse and Grabmaier, 1994). The emission from Er^{3+}-doped samples show lines that are not correlated to Er^{3+} emissions. These emissions, located around 405 and 750 nm, are associated with Fe^{3+} and Cr^{3+} impurities, respectively (Takeuchi et al., 1975). In Tm^{3+} co-doped sample, the sharp emission rays around 465 nm are assigned to $^1G_4 \rightarrow {}^3H_6$ transition of Tm^{3+} as it has been reported in $ZnS:Tm^{3+}$ and $ZnO:Li^+,Tm^{3+}$ compounds (Collins et al., 1991; Ronfard-Haret and Kossanyi, 1999), while the lines around 360 nm can be assigned to the $^1D_2 \rightarrow {}^3H_6$ transitions of Tm^{3+} (Blasse and

Grabmaier, 1994). The emission lines in the Tb^{3+}-doped samples are well-know and attributed to the indicated transitions of the Tb^{3+} ion indicated in the figure (Bos et al., 2006).

These results indicates that that Ce^{3+}, Tm^{3+}, and Tb^{3+} are entering the crystal structure and functioning as luminescence centers in the material.

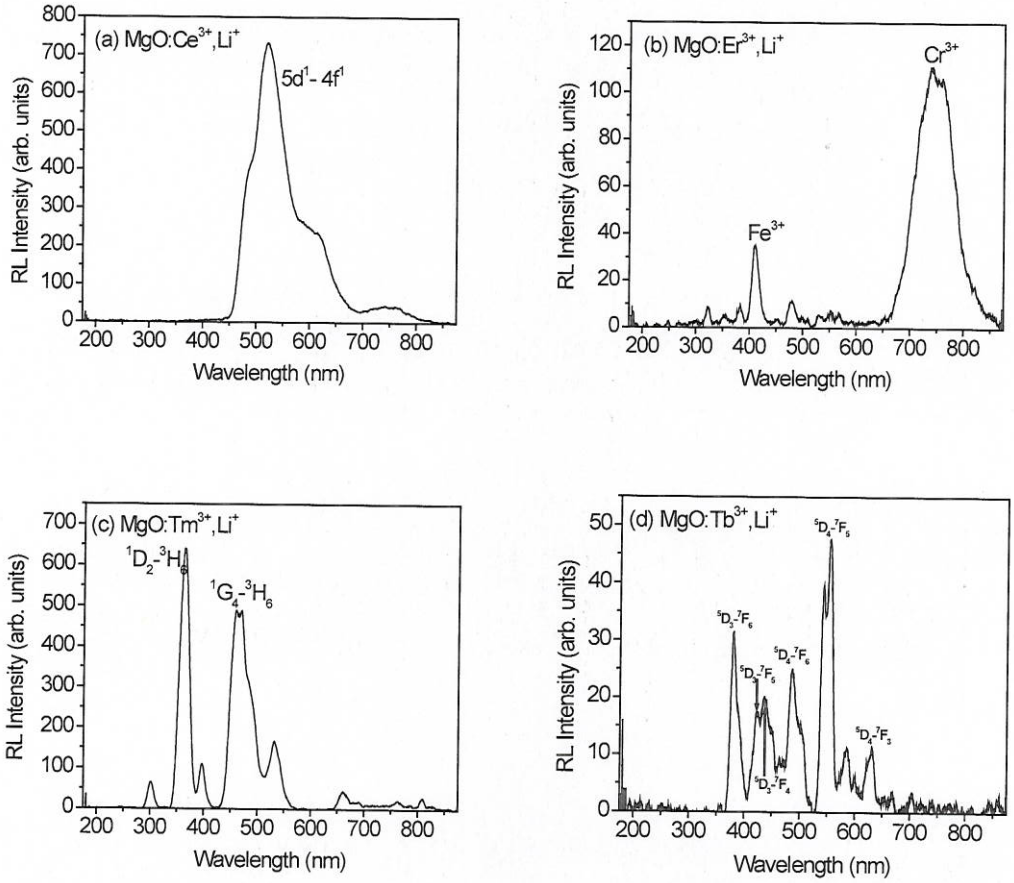

Figure 56. RL emission spectrum of MgO prepared by SCS and doped with different lanthanides (1 % molar) and Li^+ (10 % molar). The samples were annealed at 900 °C during 2 h.

Several synthesis parameters have been investigated to control and optimize luminescence processes of the ceramics produced by SCS, including:

- Combustion environment;
- Presence of co-dopants;
- Concentration of dopants.

Figure 57 compares Al_2O_3:Ce^{3+} and Al_2O_3 samples produced by SCS carried out in a hot plate and inside an oven. In both cases, the oven combustion resulted in higher TL intensity than combustion in a hot plate. We infer from these results that the better temperature uniformity in the oven increases the yield of ceramics produced. In a hot plate, the temperature gradients are

high and there is a considerable part of the material that does not reach a temperature sufficiently high to achieve a full reaction.

One of the important results in this study is the demonstration that Li^+ co-dopant can substantially increase the TL intensity of the materials being synthesized. As an example, Figure 58 shows the TL curves of $MgO:Ce^{3+}$ synthesized with or without the presence of Li^+. The Li^+ co-doped compound shows a TL intensity which is 1-2 orders of magnitude more intense than the sample produced in absence of Li^+. In addition, new TL peaks appear in the temperature range from 200-300°C. It is worthwhile to note that $MgO:Ce^{3+},Li^+$ materials exhibit several TL peaks in a large interval of temperature, as it is intended for a thermometric application.

Our most intense TL materials prepared so far, *i.e.* $MgO:Tm^{3+},Li^+$ and $MgO:Ce^{3+},Li^+$, exhibit a sensitivity comparable to commercial LiF:Mg,Ti (TLD-100) TL dosimeters (Figure 59). Although the main TL peak of Tm^{3+}-doped sample is located at too low temperature for dosimetry applications, these results are encouraging since they demonstrate the potential for producing ceramic materials with high sensitivity by SCS.

In order to check the reproducibility of SCS, two samples of $MgO:Ce^{+3}:Li^+$ were synthesized in similar conditions and their TL signal was then acquired (Figure 60). Both samples show the same TL peaks with only a slight deviation in their relative intensity and their temperature maximum which evidence that a good reproducibility via SCS technique should be achieved in the future.

Finally, quenching curves of TL and RL intensity for Al_2O_3 versus Ce^{3+} concentration in the initial solution are compared in Figure 61. A cerium concentration around 0.5% is the optimum for the TL intensity, whereas for RL the optimum concentration is around 0.2%. This difference between the two quenching optimal concentration is related to the fact that the TL process depends not only on the concentration of luminescence centers (Ce^{3+}), but also on the concentration of trapping centers in the material.

The possibility of controlling the trapping centers has not been investigated yet, but we envision to be able to control the temperature of the peaks by choice of suitable co-dopants introduced in the synthesis.

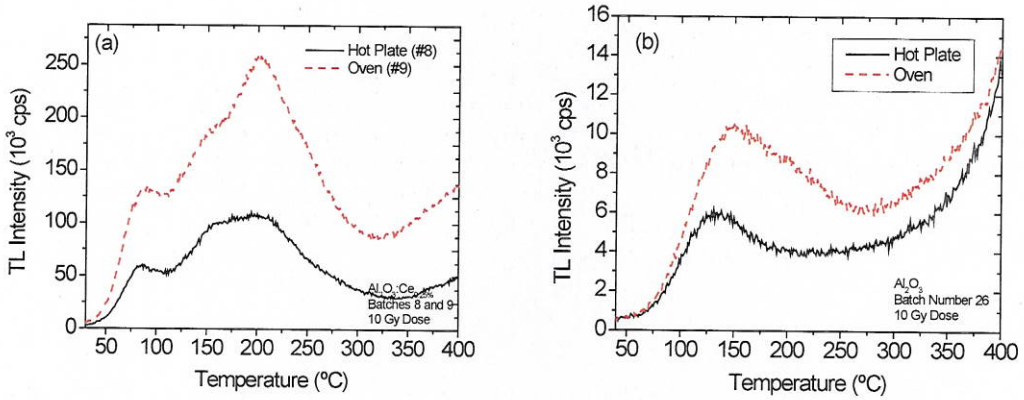

Figure 57. Comparison of TL from $Al_2O_3:Ce^{3+}$ and Al_2O_3 powder samples produced by SCS inside an oven and in a hot plate.

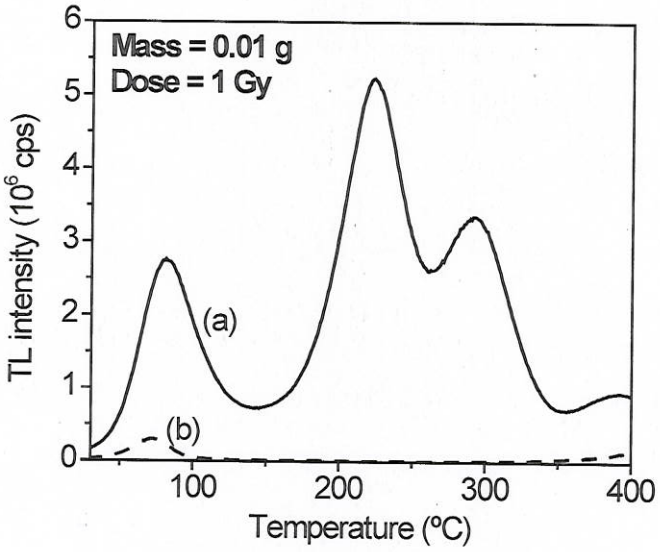

Figure 58. TL glow curves obtained after beta particle irradiation of (a) $MgO:Ce^{3+}_{(1\%)}:Li^{+}_{(10\ \%)}$and (b) $MgO:Ce^{3+}_{(0.17\%)}$. Both samples were annealed at 900 °C during 2 h.

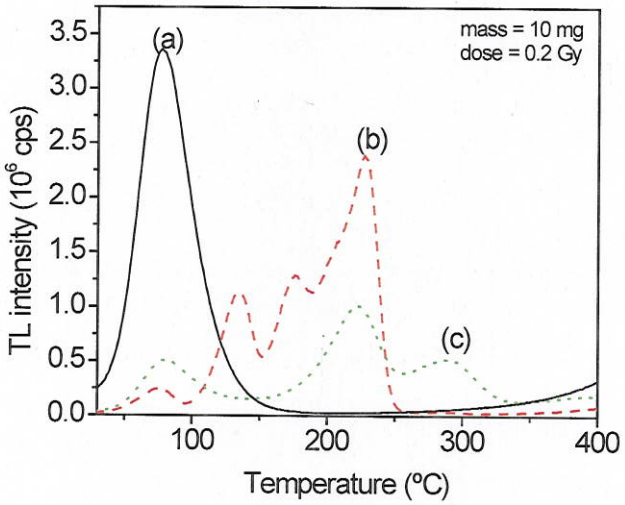

Figure 59. TL glow curves of (a) MgO:$Tm^{3+}_{(1\%)}$:$Li^{+}_{(10\ \%)}$ annealed powder sample, (b) TLD-100 powder sample and (c) MgO:$Ce^{3+}_{(1\%)}$:$Li^{+}_{(10\ \%)}$ annealed powder sample after being exposed to 0.2 Gy beta radiation (measured with 10 mg for each sample).

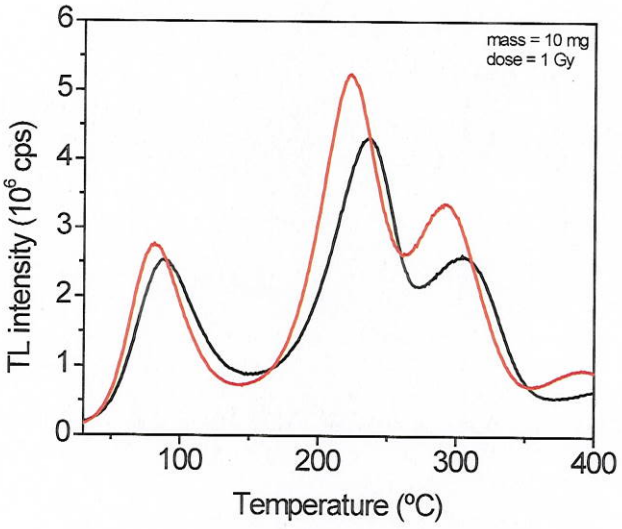

Figure 60. TL glow curves obtained after beta particle irradiation of two MgO:$Ce^{3+}_{(1\%)}$:$Li^{+}_{(10\ \%)}$ samples synthesized in the same experimental conditions.

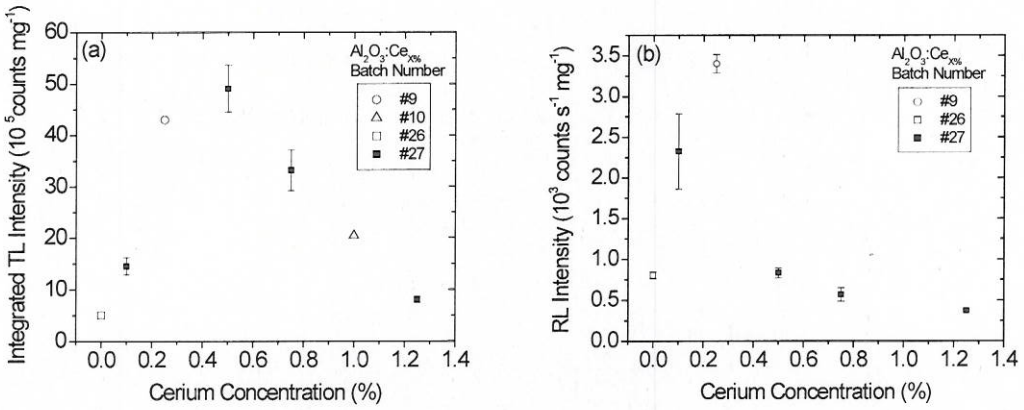

Figure 61. (a) Integrated TL intensities and (b) RL intensities of Al_2O_3:Ce samples. Each data point from batch #27 represents the average intensity of four aliquots, with error bars displaying the standard deviation of the mean. Single points have been included from previous combustions (#9, #10, and #26) which appear to be in agreement with the trend set by the behavior of batch #27. All samples were given a dose of 10 Gy prior to TL measurements.

4.6 Survivability Testing of Luminescent Particles in Explosions

The work in this section was performed in collaboration with Jim Lightstone of Indian Head Naval Surface Warfare Center.

The interior of an explosion is one of the harshest sensing environments on earth. The violent temperatures and pressures will destroy all conventional sensors, and the fireball is usually opaque to remote optical analysis due to chemistry or debris or both. However, it is still critical to know the thermal history of detonation events for applications such as the sterilization of weaponized pathogens and military explosive. We have shown earlier in this report that microparticles of thermoluminescent oxides may be used to measure temperature excursions of hundreds of degrees in tens to hundreds of milliseconds. Simulation of explosive temperatures was performed using microheaters, but these lack the severe pressure and shock stimuli which would accompany an actual explosion and so therefore could not assess the survival of luminescent microparticles in such an event.

Thermoluminescent (TL) Al_2O_3:C microparticle sensors are demonstrated to survive detonation of pentaerythritol tetranitrate (PETN) high explosives. Since TL particles have previously been shown to act as sensors for rapid high-temperature events, the stability of Al_2O_3:C particles in explosions is evaluated and several conclusions made. First, SEM imaging reveals particle features and corners with radii of curvature less than 20 μm yielding to rounded forms and increased surface roughness post-explosion. Chemical analyses by XPS and confocal Raman spectroscopy show small increases in carbon and up to a 32% decrease in aluminum on the particle surfaces, likely indicators of Al combustion. Finally, the TL emission peak and shape remain stable to within 1.9% and 4.0% respectively, less than experimental error. This means that the particle trap density-of-states and luminescence centers, and their ability to preserve thermal history information, are largely unaffected by detonation.

A high explosive charge, comprising approximately either 2 or 25 g of PETN and a detonator, was immersed in the microparticles and then triggered, as imaged in Figure 62. Particles were recovered by a plastic cone placed below the charge assembly. Chemical analysis using X-ray photoelectron spectroscopy (XPS) indicates that the explosions cause a relatively large decrease (Figure 63) in the aluminum present on the particle surfaces[2]; coupled with a smaller dip in oxygen content, this suggests the combustion of atomic aluminum. A small increase in carbon is also observed. Scanning electron microscope (SEM) examination reveals that the Al_2O_3:C microparticles, originally angular bodies with sharp corners and smooth planes (Figure 64), have been reshaped into much more rounded, compact configurations with high surface roughness (Figure 65). Most critically, the thermoluminescence glow curves of the post-explosion microparticles were collected using fresh broad-spectrum UV irradiation and compared to those of pristine microparticles. No significant difference is observed among the curves (Figure 66); the full width at half-maximum and peak location of the primary Al_2O_3:C TL peak both vary by less than the experimental error, indicating that the thermoluminescence characteristics and mechanisms of the particles have not been modified by the explosion and that their ability as thermal history sensors has therefore not been impaired.

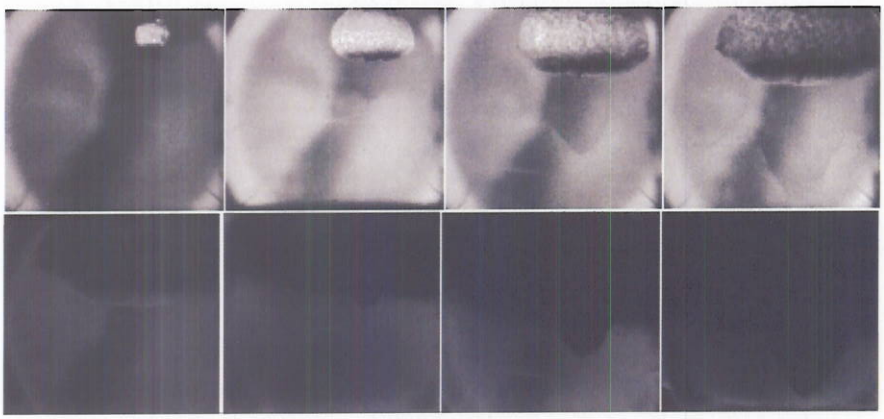

Figure 62 - The detonation of the charge + assembly in which the Al_2O_3:C microparticles were embedded. These images were captured as 20 ns exposures at 5 μs intervals.

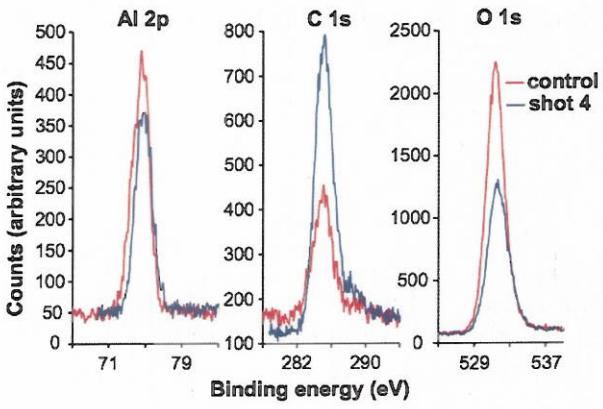

Figure 63 - High-resolution XPS spectra of Al_2O_3:C, centered on the primary peaks of its elemental constituents, after detonation of a 25 g PETN charge.

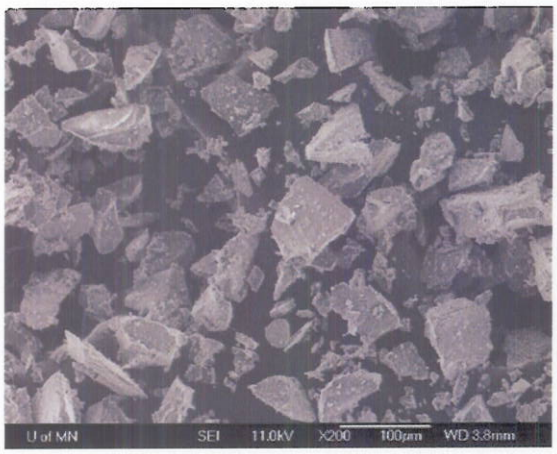

Figure 64 - SEM image of Al_2O_3:C microparticles before undergoing high explosive detonation.

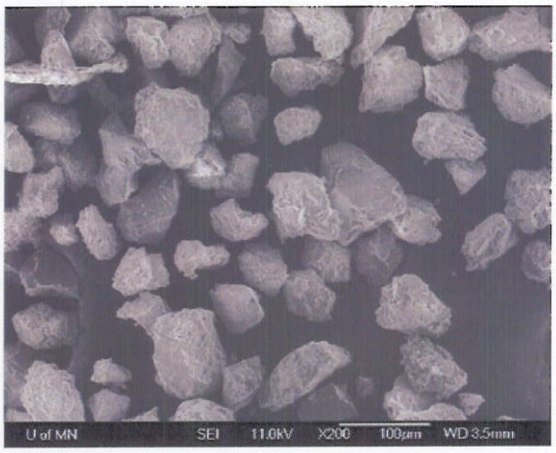

Figure 65 - SEM image of Al_2O_3:C microparticles after detonation with 25 g of pentaerythritol tetranitrate (PETN).

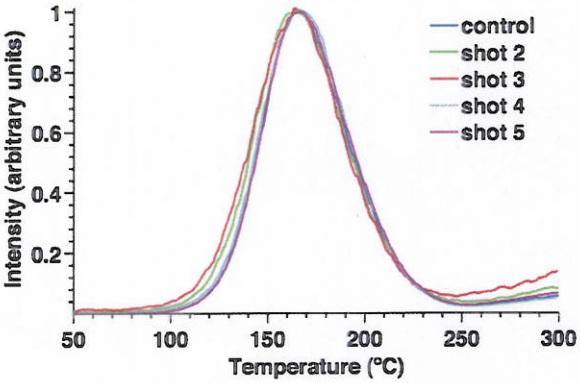

Figure 66 - Thermoluminescence glow curves of Al_2O_3:C before and after explosion with PETN charges. The data were collected using a linear heating ramp of approximately 0.9 °C/sec.

4.7 Pulsed Thermoluminescence

4.7.1 Background

Explosive heating creates significant differences in the TL compared to a standard slow heating ramp. This section will examine the scientific aspects of this. There are a number of areas of research that could benefit from the capability to perform TL measurements at heating rates orders of magnitude higher than those achievable using regular TL readers. Examples are: (i) investigation of how thermal profiles caused by detonations affect the TL of microparticles; (ii) development of techniques to perform non-destructive readout of the TL signal for radiation dosimetry. This is similar to optically stimulated luminescence (OSL)(Akselrod, 1999) (McKeever, 2003), but eliminates the need for optical filters used to discriminate between stimulation light and the material's luminescence, (iii) basic investigations on the mechanisms

related to the luminescence efficiency in TL materials; and (iv) increasing the instantaneous intensity of thermoluminescence so that small volumes of material (e.g. micro- and nano-particles) will emit signals above detector dark noise levels.

Investigation on the effect of temperature profiles generated by detonations on TL of microparticles could lead to a new method to determine the thermal profile produced by these detonations in small particles or organisms such as bacteria and spores. For this particular application, contact thermometry and stand-off methods are not able to determine the temperature profile experienced by a single particle during the entire evolution of the detonation event. Luminescence thermometry has been demonstrated using nanoparticles, but a practical application has yet to be demonstrated (Wang, 2002). Since the TL is affected by the microparticle temperature, a technique to determine the thermal profile could be developed based on the comparison of the TL of irradiated microparticles before and after the detonation. However, this requires methods to experimentally investigate the TL behavior at the fast heating rates experienced by the microparticle. For example, the temperature in a explosive-driven shock wave can vary by thousands of degrees Kelvin in a few microseconds (Davis, 1996). Therefore, it is important to develop capabilities to measure the TL at these high heating rates to compare the experimental results with computational models.

Another area of potential interest to perform fast heating rates is radiation dosimetry. Optically Stimulated Luminescence (OSL) has become widely adopted in dosimetry due to several factors. One of them is the possibility of stimulating the crystal in a very controlled way by using fast pulses of light, therefore probing the OSL signal without significantly emptying the traps responsible for the OSL signal (Akselrod, 1999). Therefore, fast heating and cooling rates could also lead to the development of a similar approach for TL dosimetry, in which the TL signal is probed using short thermal pulses without emptying significantly the associated traps, as proposed earlier. One of the advantages would be to eliminate the need for optical filters used in OSL to discriminate between stimulation light and the material's luminescence.

In this section, we describe a pulsed thermoluminescence (PTL) technique where short voltage pulses are applied to a resistor on a microheating stage. The stage heats and then cools rapidly, transferring energy to one or more luminescent particles on the stage, exciting trapped carriers which recombine and produce light. The technique is demonstrated using particles of α-Al_2O_3:C, which is a common TL and OSL dosimetric material.

4.7.2 Procedure

Two types of heaters were fabricated: one set was etch-released from the substrate and had slow time constants (~50ms); the other set was not etch-released and had fast time constants (less than 500μs). These latter microheaters consisted of silicon nitride plates with platinum resistors used for joule heating. The temperature of the heaters was determined by measuring the change in resistance as the structure was heated.

Platinum was chosen for the resistors since the temperature coefficient of resistance (TCR) is constant up to temperatures near 600°C (Firebaugh, 1998). The TCR of the platinum resistor was determined by measuring the resistance of the device as it was heated on a hot plate up to 90°C. The resistance versus temperature was linear over the entire measurement range and was assumed to be linear beyond 90°C. We calculated the temperature change as a function of

applied power for different pulse lengths by measuring the resistance change during a voltage pulse. The temperature of the resistors was calculated using the formula:

$$\Delta T = \left(\frac{R}{R_o} - 1 \right) \Big/ \alpha \qquad (1)$$

Where ΔT is the change in temperature, R the resistance during heating, R_o the resistance at room temperature and α is the TCR of the material.

To measure the luminescence, the photon counts were recorded with a photomultiplier tube for one second. This time period was chosen since it was much longer than the luminescent lifetime of Al_2O_3:C and thus collected essentially all the photons from a single pulsed excitation. The temperature pulse occurred immediately after the photon count had started, which allows one to assign the total integrated intensity to the single pulse.

Immediately after this measurement was recorded, a background measurement was taken for one second. This verified that there was no residual luminescence remaining after the initial measurement. Changes in this measurement were never observed confirming that one second was long enough to record all the thermoluminescence due to a pulse.

To prepare the Al_2O_3:C for PTL measurements, a single particle was placed on a microheater. The same particle was used for all measurements and was approximately 80-100μm in diameter. Its size was estimated by comparing it to the size of the heater plate. To empty the traps before exposure, the particle was heated repeatedly to 250°C for 50 ms until the measured light intensity was equal to the background level. The traps were then filled by exposing the particle to 205nm light for 20 min. This wavelength coincides with the absorption band of F-centers in Al_2O_3. The UV photons create free electrons that can be trapped at defects in the crystal (Lee, 1979).

There were two different methods used for taking PTL measurements. The first method was temperature ramping PTL (TR-PTL), where the peak temperature of each pulse was increased by a constant amount over that of the previous pulse. This allowed the measurement to be displayed in a plot of photon count versus temperature.

The second method was constant temperature PTL (CT-PTL). In this technique, the temperature was pulsed repeatedly at the same level, and the data was plotted in a graph of photon count verses pulse number. This allowed the change in trap population to be examined as a function of pulse number.

The results were interpreted according to the first-order TL model, in which the probability of a charge escaping from the trap per unit time is given by:

$$p = se^{-E/kT} \qquad (2)$$

and the TL intensity I is given by the rate of change in the trapped charge population:

$$I = -\frac{dn}{dt} = np \qquad (3)$$

In these equations, E is the activation energy for the process, s is the frequency factor or pre-exponential factor, k is the Boltzmann constant, T is the temperature, and n is the concentration of trapped charges. It is understood that first order kinetics are not a perfect quantitative representation for Al_2O_3:C luminescence because of quenching at higher temperatures (Akselrod, 1999) but this approximation provides a simple model to understand the qualitative behavior of the system and demonstrate the potential of PTL. The intensity as a function of temperature for a standard TL ramp is given by:

$$I(T) = n_0 s e^{-E/kT} \exp\left[-\frac{s}{\beta}\int_{T_0}^{T} e^{-E/k\theta} d\theta\right] \qquad (4)$$

where β is the heating rate and T_o the initial temperature of the sample. The TL emitted during the *i*th thermal pulse in a TR-PTL or CT-PTL measurement for a pulse durationΔt and initial trap population of n_i is given by the integral of (3):

$$\int I dt = n_i\left(1 - \exp\left[-\Delta t \cdot s e^{-E/kT_i}\right]\right) \qquad (5)$$

The surviving concentration of trapped charges after a thermal pulse is then:

$$n_{i+1} = n_i \exp\left[-\Delta t \cdot s e^{-E/kT_i}\right] \qquad (6).$$

If

$$1 >> \exp\left[-\Delta t \cdot s e^{-E/kT_i}\right] \qquad (7)$$

then the detrapping is small between pulses and the intensity remains near constant for all pulses.

4.7.3 Data from Pulsed Thermoluminescence Experiments

In Figure 67 the TR-PTL curve is plotted for both 50 and 10 ms pulses as curves 67b and 67c respectively. Each point corresponds to the integrated luminescence measurement from one pulse. Curve 67a is a standard TL curve of α-Al_2O_3:C using a heating rate of 5 K/s and is added for comparison. The temperatures listed are of the platinum thermistor. Note that the TR-PTL peaks have a similar shape to a standard TL curve but are shifted to higher temperatures. The positions of the peaks were seen to increase with decreasing pulse length. Also, the temperature of the onset of luminescence is observed to increase with decreasing pulse length.

Figure 68 is a plot of CT-PTL. The curves appear to decay exponentially with pulse number. However, for small temperatures the decay is slow enough that the intensity is nearly constant over a large number of pulses. Also, the intensity was observed to increase with the temperature of the pulse.

4.7.4 Discussion

The observed temperature shift in the TR-PTL curves when compared to the standard TL curve has two causes. First, the overall amount of energy delivered to the heater by the time a certain temperature is reached differs depending on the heating rate. The time required for a heater to reach a temperature of 500K from room temperature at a heating rate of 1 K/s is twice that using a heating rate of 2 K/s. Clearly, more energy is delivered to a heater in the first case. This means that more traps will be excited at lower temperatures in the slow ramp, shifting the peak luminescence lower in temperature. This dependence of the TL peak position on the heating rate is very well-known and applies equally to rapid pulses. A TL curve obtained using a heating rate of 5 K/s should show peak luminescence at a much lower temperature than a TL curve produced using a series of 10 ms square pulses with gradually increasing amplitude. Likewise, a series of similarly increasing 50ms square pulses should lead to a TL curve intermediate between the two. This is the behavior measured in Figure 67 and modeled in Figure 69 using first order kinetics.

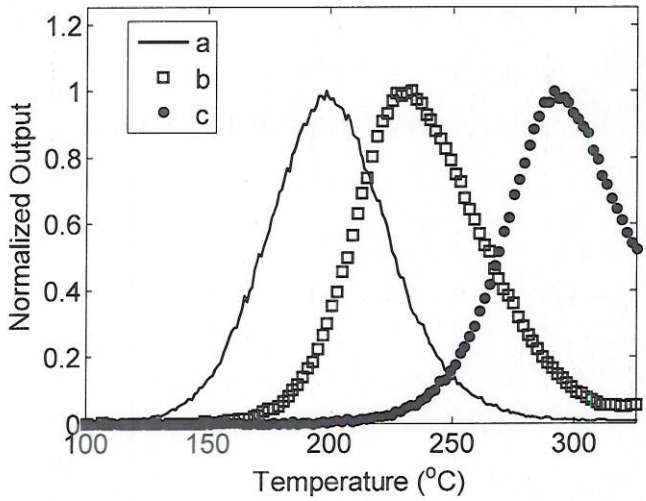

Figure 67: Curves for Al_2O_3:C a) intensity of a standard TL curve. Heating rate 5°C/s. b) Integrated intensity due to a pulse in a PTL curve. 50 ms pulses, 2°C increase per pulse. c) Integrated intensity in a PTL curve. 10 ms pulses, 2°C increase per pulse.

The second possible reason for shifts in the luminescence is due to the imperfect thermal contact between the particles and the heaters. This leads to a delay in heat transfer from heater to particle. If the delay is longer than the pulse time, the particle would never able to reach the expected temperature. One may be seeing the beginnings of the effect by the larger separation between the 50 ms and 10 ms peaks in the measured data over the simulations. Based on the

close match between Figures 67 and 69, this appears to be a secondary effect that could be eliminated by using deposited thin films on microheaters as luminescent materials.

The potential use of PTL to allow a dosimetric material to be read repeatedly can be seen in Figure 68. At lower temperatures CT-PTL is near constant over many pulses. This indicates the luminescence can be read multiple times from the same particle without losing stored information about the population of traps.

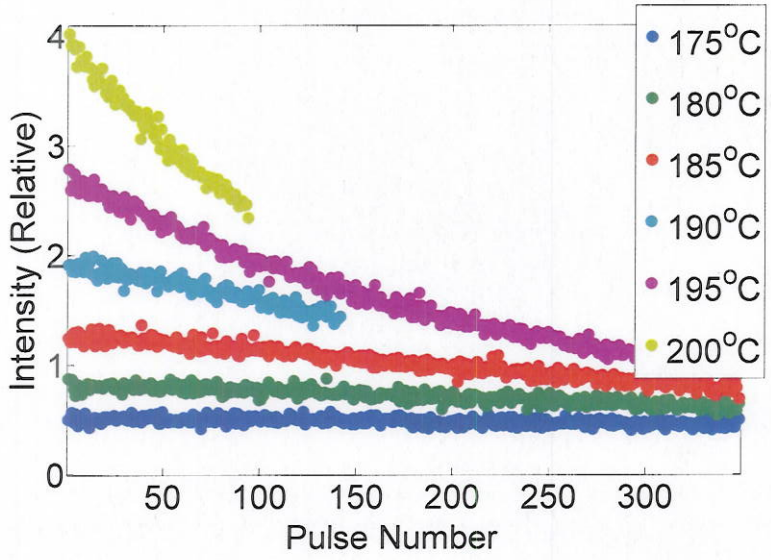

Figure 68: PTL at constant temperature. The pulse length was 50 ms. The temperatures of the pulses for different curves were 175, 180, 185, 190, 195 and 200°C.

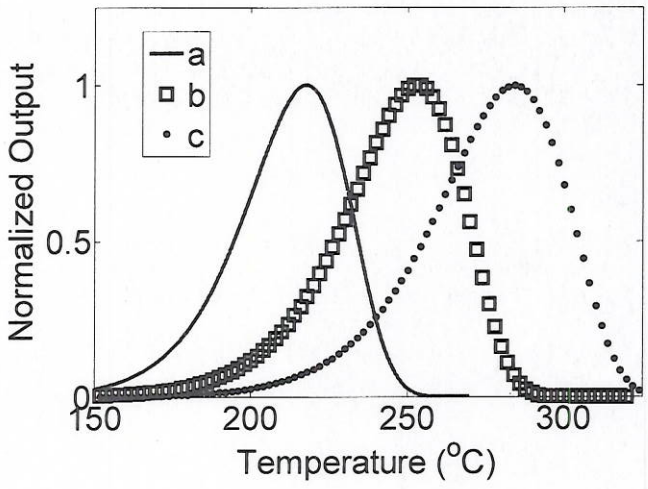

Figure 69: Simulation first order curves for: a) TL 5 °C/s b) TR-PTL 50ms c) TR-PTL 10ms. This data is not expected to exactly match that of Figure 2 because α-Al_2O_3:C is not an ideal material with first-order kinetics, but the qualitative shift is seen to be very similar.

The use of PTL may also be a helpful technique in decreasing the effects of thermal quenching in luminescent particles as well as potentially investigate the thermal quenching mechanism. For this to be a viable option, the thermal time constant of the microheater-plus-TL-material would have to be much less than the F-center lifetime (35 ms at room temperature) (Akselrod, 1999) Then by applying temperature pulses shorter than the F-center lifetime, the majority of the decay can occur at room temperature where the signal is not affected by thermal quenching. Since the heaters in this study have time constants on the order of 500μs, these studies will be possible by matching the thermal mass of the TL material with improved thermal contact, such as would be obtained using deposited thin films.

The technique of PTL could also be used in an integrated badge dosimeter which would be able to warn the user if they had received a harmful amount of radiation. The device could consist of a TL particle, microheater and avalanche photodiode. Since an avalanche photodiode tends to be noisier than a PMT, a single PTL pulse could potentially be used to increase the intensity of emitted light above the noise level of the photodiode in a single temperature pulse. Although in our work we were unable to test this due to equipment limitations, this can be anticipated to increase the intensity of the signal by imagining a pulse at the same temperature as the peak of a standard TL curve. The luminescent efficiency and rate of trap emptying would be the same in both cases. However, with a single temperature pulse, there was no previous emptying of traps at lower temperatures like there would be with a standard TL ramp. Since there would be a greater number of filled traps, the intensity is anticipated to be greater.

5 CONCLUSIONS

Construction of a thermoluminescence system with controlled explosive-rate heating and cooling:

- Microheaters for simulating explosive temperatures in microparticles have been completed. Various sorts of microheaters have fabricated. The fastest, for rapid heating can ramp to 350°C with time constants of a few hundred microseconds with equally fast cooling rates. Other heaters have been fabricated with maximum temperatures that can exceed 800°C but with time constants in the tens of milliseconds.
- A thermoluminescence system has been constructed, tested, and verified that simulates explosive heating without confounding pressure effects. The entire process from UV excitation for trap filling of microparticles to data processing of TL data has been fully automated for both standard TL and explosive heating.

Demonstration of basic thermometry concept:

- Basic modeling to extract both maximum temperature and cooling time has been performed. Modeling of the luminescence with ramp speed and pulse energy was completed. Simulations show that obtaining the peak temperature that a particle has

reached is relatively straightforward in theory but information on cool-down is more difficult but not impossible. The important parameters of the microparticles are trap depth and lattice (phonon) interaction time. Using multiple particles is necessary in principle to isolate maximum temperature and cooling time.

- Using experimental and numerical studies based on LiF:Mg,Ti, it was demonstrated that a superposition of first-order TL peaks offers more information than a single TL peak. We showed that two different profiles that would result in the same change of a single TL peak (e.g. a fast heating to a high temperature *versus* a slow heating to a lower temperature) would affect differently other TL peaks in the material, therefore opening the possibility of distinguishing the heating profiles based on the superposition of TL peaks.

- The core concept of the program of using microparticle TL to extract maximum temperature with rapid heating rates and slower cooling times, mimicking what would be seen in an agent defeat test. $MgSiO_4$:Co,Tb and Al_2O_3:C microparticles were used with microheater excitation. Peak temperatures were recovered with good accuracy. The peak temperatures ranged from 232 °C to 313 °C with durations less than 200ms. The observed change in the thermoluminescence peak intensity ratio of two Mg_2SiO_4:Tb,Co traps has been predicted with an average error of 4.4% using first-order kinetics modeling.

- In the process of creating explosive heating, we discovered a new characterization technique, pulsed thermoluminescence, that that enables one to assess the trap population using a single or series of pulses. This may allow single particles to have an instantaneous thermoluminescent intensity that is higher than standard TL, enabling the read-out of very small particles, which is particularly important for luminescent thermometry.

Characterization of existing dosimetric materials for thermometry:

- Existing materials are available with properties that could be used as a temperature sensor. LiF:Mg,Ti emerged as the most favorable material due to its high TL intensity, presence of several TL peaks, and agreement between experimental data obtained using this material and simulations using TL models.

- One of the predominant problem for the use of existing TL materials in temperature sensing is the light sensitivity of the trapping centers. Except for LiF:Mg,Ti and natural topaz, all other materials show some degree of light sensitivity.

- Investigation of new nanophosphors produced by Solution Combustion Synthesis (SCS) indicate a possible new route for material synthesis. The oxyorthosilicates investigated in this study were not suitable for temperature sensing because of the low TL intensity, but this does not exclude the possibility of using SCS to produce other materials with desirable properties.

Development of new materials for luminescence thermometry:

- The possibility of synthesizing TL materials using the Solution Combustion Synthesis (SCS) technique was demonstrated. Materials were produced with favorable TL properties, i.e., several TL peaks and emission bands corresponding to the emission from dopants introduced. However, this is a new field of development in TL research which will require substantial effort before the materials can be properly engineered with the desired properties.

6 REFERENCES

Akselrod, M. S. and McKeever, S. W. S. A radiation dosimetry method using pulsed optically stimulated luminescence. Radiat. Prot. Dosim. 81, 167-176 (1999).

Bapat, M.N. and Sivaraman, S., 1986. *Temperature dependence of luminescence emission from cerium and europeium doped MgO under x-ray excitation*. Pramana - J. Phys. 27, 813-820.

Benoit P. H., D. W. G. Sears, and S. W. S. McKeever, "The natural thermoluminescence of meteorites: II. meteorite orbits and orbital evolution," Icarus, vol. 94, no. 2, pp. 311–325, Dec. 1991.

Blasse, G. and Grabmaier, B.C., 1994. *Luminescent materials*. Springer, Heidelberg.

Bos, A.J.J., Prokić, M. and Brouwer, J.C., 2006. *Optically and thermally stimulated luminescence characteristics of MgO:Tb^{3+}*. Radiat. Prot. Dosim. 119, 130-133.

Chen, R. and McKeever, S.W.S., 1997. *Theory of thermoluminescence and related phenomena*. World Scientific Publishing Co., Singapore.

Chick, L.A., Pederson, L.R., Maupin, G.D., Bates, J.L., Thomas, L.E. and Exarhos, G.J., 1990. *Glycine-nitrate combustion synthesis of oxide ceramic powders*. Mater. Lett. 10, 6-12.

Collins, B.T., Kane, J., Ling, M., Tuenge, R.T. and Sun, S.-S., 1991. *Preparation and photoluminescence of thulium-activated zinc sulfide films*. Journal of Electrochemical Society 138, 3515-3518.

Davis, L. L. and Brower, K. R. Reactions of Organic Compounds in Explosive-Driven Shock Waves. J. Phys. Chem. 100, 18775-18783 (1996).

Escobar-Alarćon L., E. Villagrán, E. Camps, S. Romero, J. E. Villarreal-Barajas, and P. R. González, "Thermoluminescence of aluminum oxide thin films subject to ultraviolet irradiation," Thin Solid Films, vol. 433, no. 1-2, pp. 126–130, 2003.

Firebaugh S. L., K. F. Jensen and M. A. Schmidt, Investigation of High-Temperature Degradation of Platinum Thin Films with an *In Situ* Resistance Measurement Apparatus. J. Microelectromech. Syst. 7, 128-135 (1998)

Furetta C., Handbook of Thermoluminescence. Singapore: World Scientific Publishing, 2003.

Kingsley, J.J. and Patil, K.C., 1988. *A novel combustion process for the synthesis of fine particle α-alumina and related oxide materials*. Mater. Lett. 6, 427-432.

Kingsley, J.J., Manickam, N. and Patil, K.C., 1990. *Combustion syntehsis and properties of fine particle fluorescent aluminous oxides*. Bull. Mater. Sci. 13, 179-189.

Kruse P. W. , L. D. McGlauchlin, and R. B. McQuistan, Elements of Infrared Technology. New York: John Wiley & Sons, 1962.

Lee, K. H. and Crawford Jr., J. H. Luminescence of the F center in sapphire. Phys. Rev. B 19 (6), 3217-3221 (1979).

McKeever S. W. S. and D. W. Sears, "The natural thermoluminescence of meteorites: A pointer to meteorite orbits?" Modern Geology, vol. 7, pp. 137–145, 1980.

McKeever, S.W.S., 1985. *Thermoluminescence of solids*. Cambridge University Press, Cambridge.

McKeever, S.W.S., Moscovitch, M. and Townsend, P.D., 1995. *Thermoluminescence dosimetry materials: properties and uses*. Nuclear Technology Publishing, Ashford.

McKeever, S. W. S. and Moscovitch, M. On the advantages and disadvantages of optically stimulated luminescence dosimetry and thermoluminescence dosimetry. Radiat. Prot. Dosim. 104, 263-270 (2003).

Mittani J. C. , M. Prokić, and E. G. Yukihara, "Optically stimulated luminescence and thermoluminescence of terbium-activated silicates and aluminates," Radiation Measurements, vol. 43, no. 2-6, pp. 323–326, Jun. 2008.

Randall, J.T. and Wilkins, M.H.F., 1945. *Phosphorescence and Electron Traps. I. The Study of Trap Distributions*. Proc. Roy. Soc. A 184, 365-389.

Ronfard-Haret, J.C. and Kossanyi, J., 1999. *Electro- and photoluminescence of the Tm^{3+} ion in Tm^{3+}- and Li^{+}-doped ZnO ceramics. Influence of the sintering temperature*. Chem. Phys. 241, 339-349.

Sears D. W. and A. A. Mills, "Thermoluminescence and the Terrestrial Age of Meteorites," Meteoritics, vol. 9, pp. 47–67, 1974.

Takeuchi, N., Inabe, K. and Nanto, H., 1975. *Effect of iron impurity concentration on kinetics order of thermoluminescent blue emission in MgO single crystals*. Solid State Commun. 17, 1267-1269.

Wang S. and Chen, W. Nanoparticle luminescence thermometry. Journal of Physical Chemistry B 106, 11203-11209 (2002).

Wintle, A. G. and D. J. Huntley, "Thermoluminescence dating of a deep sea sediment core," Nature, vol. 279, no. 5715, pp. 710–712, Jun. 1979.

Yen, W.M. and Weber, M.J., 2004. *Inorganic Phosphors: Compositions, Preparation and Optical Properties*. CRC Press, Boca Raton.

Yukihara, E.G. and Okuno, E., 1998. *On the thermoluminescent properties and behavior of Brazilian topaz*. Nucl. Instr. Meth. Phys. Res. B 141, 514-517.

DEPARTMENT OF DEFENSE

DEFENSE TECHNICAL
INFORMATION CENTER
8725 JOHN J. KINGMAN ROAD,
SUITE 0944
FT. BELVOIR, VA 22060-6201
ATTN: DTIC/OCA

EXELIS, INC.
1680 TEXAS STREET, SE
KIRTLAND AFB, NM 87117-5669
ATTN: DTRIAC